DEUTSCHE
BUNDESBANK
EUROSYSTEM

Discussion Paper

Deutsche Bundesbank
No 32/2026

Some thoughts on modified X-11 seasonal adjustments for time series with complex seasonality

Karsten Webel

Discussion Papers represent the authors' personal opinions and do not necessarily reflect the views of the Deutsche Bundesbank or the Eurosystem.

Editorial Board: Daniel Foos
Stephan Jank
Thomas Kick
Martin Kliem
Malte Knüppel
Christoph Memmel
Hannah Paule-Paludkiewicz

Deutsche Bundesbank, Wilhelm-Epstein-Straße 14, 60431 Frankfurt am Main,
Postfach 10 06 02, 60006 Frankfurt am Main

Tel +49 69 9566-0

Please address all orders in writing to: Deutsche Bundesbank, Press and Public Relations Division, at the above address or via email: www.bundesbank.de/contact

Internet http://www.bundesbank.de

Reproduction permitted only if source is stated.

DOI https://doi.org/10.71734/DP-2026-32
ISBN 978-3-98848-091-0
ISSN 2941-7503

Some thoughts on modified X-11 seasonal adjustments for time series with complex seasonality*

Karsten Webel
Deutsche Bundesbank

Abstract

A recent release of the JDemetra+ time series software for official statistics implements a modification of the classical X-11 seasonal adjustment approach for monthly and quarterly data. Although this modified method can handle seasonal data with any periodicity, it has been specifically designed to accommodate peculiarities typically seen in time series recorded at sub-monthly intervals. The main novelty is the implementation of rich families of kernel-based trend-cycle extraction filters that encompass the traditional Henderson and Musgrave filters, so that the modified X-11 method is essentially a hybrid switching iteratively between parametric trend-cycle estimation and nonparametric seasonal estimation. Notwithstanding these enhancements, the X-11 modifications also implement some simplifications of the classical routines, which mainly concern automatic detection and selection procedures. Consequently, the current maturity level of the modified computing routines is unclear. We therefore catalogue the conceptual differences between the two X-11 methods and assess their ramifications empirically, using real-time data on monthly production of capital goods in Germany under different seasonal adjustment settings in a concurrent revision regime. Given the multitude of options for parametric trend-cycle estimation, we also seek to find out whether different trend-cycle filter configurations provoke significant discrepancies in final estimated signals. To this end, we consider real-time weekly Google trends as well as daily electricity consumption in Germany and evaluate various quality criteria, such as the stability of the data-driven selection of seasonal filters, the systematic occurrence of issues related to remaining seasonal autocorrelation, and the revision profiles of concurrent seasonally adjusted estimates.

Keywords: JDemetra+, kernel-based trend-cycle estimation, local polynomial regression filters, reproducing kernel Hilbert spaces, real-time data, revision analysis.

JEL classification: C01, C02, C14, C22, C40, C50.

*Contact address: Karsten Webel, Deutsche Bundesbank, Central Office, Directorate General Data & Statistics and Research Centre, Postfach 10 06 02, 60006 Frankfurt am Main, Germany. Phone: +49 69 9566 32702. E-mail: karsten.webel@bundesbank.de. The author thanks Alessandra Luati and Jean Palate for valuable comments. Discussion papers represent the authors' personal opinions and do not necessarily reflect the views of the Deutsche Bundesbank or the Eurosystem.

1 Motivation

Starting with the inaugural release from its third version branch in May 2023, the JDemetra+ (JD+) software for time series econometrics in official statistics contains, among many other new features, a modification of the famous X-11 seasonal adjustment method for monthly and quarterly time series (Shiskin, Young, and Musgrave, 1967). The development of such modified methods has been predominantly triggered by the urgent need to process daily and weekly data for the timely monitoring of the economic turbulence in the wake of the COVID-19 pandemic outbreak in Q1 2020. Nevertheless, this particular X-11 modification is generally applicable to seasonal time series with any periodicity and any number of superimposed seasonal patterns, see, for example, the preparatory considerations in Ladiray, Palate, Mazzi, and Proietti (2018) as well as the overviews in Webel (2022) and Webel and Smyk (2024).

The most remarkable addition to the modified X-11 method is undoubtedly the augmented set of linear filters for trend-cycle extraction. Whereas the classical X-11 method relies on composite simple moving averages at the preliminary filtering stages and on Henderson filters (with hard-coded weights) at the refined and final filtering stages, the modified X-11 method utilises generalised composite moving averages and rich kernel-based filter families, derived either from local polynomial regression models (Proietti and Luati, 2008) or from reproducing kernel Hilbert spaces (Aronszajn, 1950). Encompassing the classical Henderson filters and their asymmetric Musgrave surrogates as special cases, either framework provides a wide range of options for specifying trend-cycle filters, including the constituent kernel, the polynomial trend degree to be preserved, and the way asymmetric filters should be derived from symmetric filters. The modified X-11 method can thus be seen as an iterative linear filtering technique that combines parametric trend-cycle estimation with nonparametric *ad hoc* seasonal estimation. From a conceptual point of view, it thus blends in with previous research on hybrid signal extraction approaches, such as the iterated Wiener-Kolmogorov filter for additive latent components models (McElroy and Sutcliffe, 2006) and a model-based X-11 variant for multiplicative latent components models (McElroy, 2010).

These eye-catching enhancements, however, come at the cost of some simplifications, mostly with respect to the automatic detection and selection procedures of the classical X-11 method. For example, the modified computing routines lack the data-driven selection of trend-cycle and seasonal filters, the built-in replacement of extremes in the detrended series before the final seasonal estimation in the last filtering stage, and the opportunity to configure different seasonal filters for different periods. One is thus tempted to ask if the availability of enhanced parametric methods for kernel-based trend-cycle estimation actually outweighs the aforementioned, and other, conceptual limitations. The present paper therefore attempts to shed some light on the current maturity status of the modified X-11 method by delivering an exhaustive technical documentation of the changes made to the classical computing routines and by tackling empirically the following two sub-items:

1. How closely can selected benchmark signal estimates, obtained with the classical X-11 method, be replicated with the modified X-11 routines?

2. Do different configurations of the kernel-based trend-cycle filter in the modified X-11 method result in significantly different final seasonally adjusted estimates?

Section 2 reviews the basic principles of the classical X-11 filtering philosophy and provides an exhaustive list of the conceptual changes introduced into the recent modification. This documentation is mostly non-technical, as the mathematical foundation of the kernel-based frameworks for parametric trend-cycle estimation is described in the Appendix, extending the previous exposition given in Webel and Smyk (2024). Section 3 deals with our first sub-item. We consider monthly real-time industrial production data for Germany to compare selected outcomes of concurrent classical and modified X-11 seasonal adjustments. To this end, the latter method will utilise trend-cycle extraction filters based upon the exact Henderson and biweight kernels with short bandwidths under the classical Musgrave boundary assumptions. Section 4 is concerned with our second sub-item. We look at real-time data on weekly Google searches for unemployment and daily realised electricity consumption in Germany to evaluate the quality of the concurrent seasonally adjusted vintage series obtained with the modified X-11 method under different settings for kernel-based trend-cycle estimation. Our quality assessment covers the stability of the data-driven selection of seasonal filters based upon a redesigned moving seasonality ratio (Webel, 2026), the presence of consistent seasonal adjustment inadequacies with respect to remaining seasonal autocorrelation, and the size and volatility of both short- and long-term revisions. Focusing on trend-cycle filters with longer bandwidths, this empirical study will include all available kernels and derivation concepts for finding asymmetric boundary filters. It thus elaborates a recent revision analysis that utilised only the exact Henderson kernel under one specific boundary scenario (Webel, 2025). Finally, Section 5 summarises the main findings and concludes with some suggestions for further research.

2 Basics of X-11 seasonal adjustments

2.1 Classical method

Let $\{y_t\}$ denote a time series with τ observations per year. The classical X-11 method, originally developed by Shiskin et al. (1967), is a nonparametric seasonal adjustment approach for monthly and quarterly time series, so we temporarily assume $\tau \in \{4, 12\}$. We also accept the traditional notion that $\{y_t\}$ can be decomposed additively, maybe after taking logs, into four unobservable components (UC) according to

$$y_t = t_t + s_t + c_t + i_t, \tag{1}$$

where

- $\{t_t\}$ is the trend-cyclical component capturing the long-term evolution of the series,
- $\{s_t\}$ is the (single) seasonal component covering repetitive sub-annual movements that recur each year in the same season with similar intensity,
- $\{c_t\}$ is the calendar component absorbing long-term periodic variation related to the varying number of trading or working days, as well as to the dates of moving holidays, and
- $\{i_t\}$ is the irregular component collecting all the remaining short-term dynamics of the series.

We now sketch how X-11 literally produces estimates of these components. Additions to and refinements of the original method, including mathematical details, can be found in Findley, Monsell, Bell, Otto, and Chen (1998) and in a step-by-step walk through the various X-11 output tables (Ladiray and Quenneville, 2001).

Section A: data linearisation Prior to the estimation of the trend-cyclical, seasonal, and irregular components, the observed time series is usually cleaned from deterministic movements associated with certain types of outliers and with the calendar component $\{c_t\}$ in model (1). This is typically done with the aid of a linear time series regression with autoregressive integrated moving average (ARIMA) disturbances, which can be written compactly as

$$\phi_p(L)\Phi_P(L^\tau)(1-L)^d(1-L^\tau)^D\left(y_t - \mathbf{x}_t^\top\boldsymbol{\beta}\right) = \theta_q(L)\Theta_Q(L^\tau)\,\varepsilon_t, \tag{2}$$

where L is the lag operator, i.e. $Ly_t = y_{t-1}$, $\mathbf{x}_t$ is a vector of exogenous regression variables, $\boldsymbol{\beta}$ is a vector of unknown regression coefficients, $\phi_p(L)$ and $\Phi_P(L^\tau)$ are nonseasonal and seasonal autoregressive (AR) polynomials of finite orders p and P, respectively, d and D are the orders of nonseasonal and seasonal differencing, $\theta_q(L)$ and $\Theta_Q(L^\tau)$ are nonseasonal and seasonal moving average (MA) polynomials of finite orders q and Q, respectively, and $\{\varepsilon_t\}$ is zero-mean white noise with finite variance. We shall use the short-form notation $(pdq)(PDQ)_\tau$ to refer to a specific version of model (2).

Both the ARIMA orders and the outliers can be specified by the user or be identified automatically, using the algorithms described in Gómez and Maravall (2001). Either way, an estimate of the calendar component in model (1) is finally obtained from the fitted pretreatment model via $\hat{c}_t = \mathbf{x}_{t,c}^\top\hat{\boldsymbol{\beta}}_c$, with $\mathbf{x}_{t,c}$ and $\boldsymbol{\beta}_c$ denoting the subvectors of $\mathbf{x}_t$ and $\boldsymbol{\beta}$ that contain the calendar-related regression variables and coefficients, respectively.

Sections B through D: UC estimation Leaning on the "ratio-to-moving-average" principle (Macaulay, 1931), the core idea of the classical X-11 method is to run a predetermined sequence of linear filtering operations on the linearised time series to produce a sequence of preliminary, refined, and final estimates of the trend-cyclical, seasonal, and irregular components from model (1). This sequence is schematised in Figure 1 and essentially boils down to a repeated application of the following 4-step principle:

1. Obtain an estimate of the trend-cyclical component by smoothing the input series with a proper trend-cycle filter. Both the input series and the type of trend-cycle filter depend on the current position in the entire filtering process (see below).

2. Remove the estimated trend-cycle from the observed time series to obtain an estimate of the fused seasonal-irregular component.

3. Obtain estimates of the seasonal and irregular components by period-wise smoothing the seasonal-irregular component either with a composite $3 \times k$ seasonal moving average, which admits the polynomial representation

$$\mathcal{S}_{3\times k}(L) = \mathcal{S}_3^\star(L)\,\mathcal{S}_k^\star(L) \quad \text{with} \quad \mathcal{S}_m^\star(L) = \frac{1}{m}\,\frac{L^{\tau m}-1}{L^\tau - 1}\,L^{-\tau(m-1)/2}$$

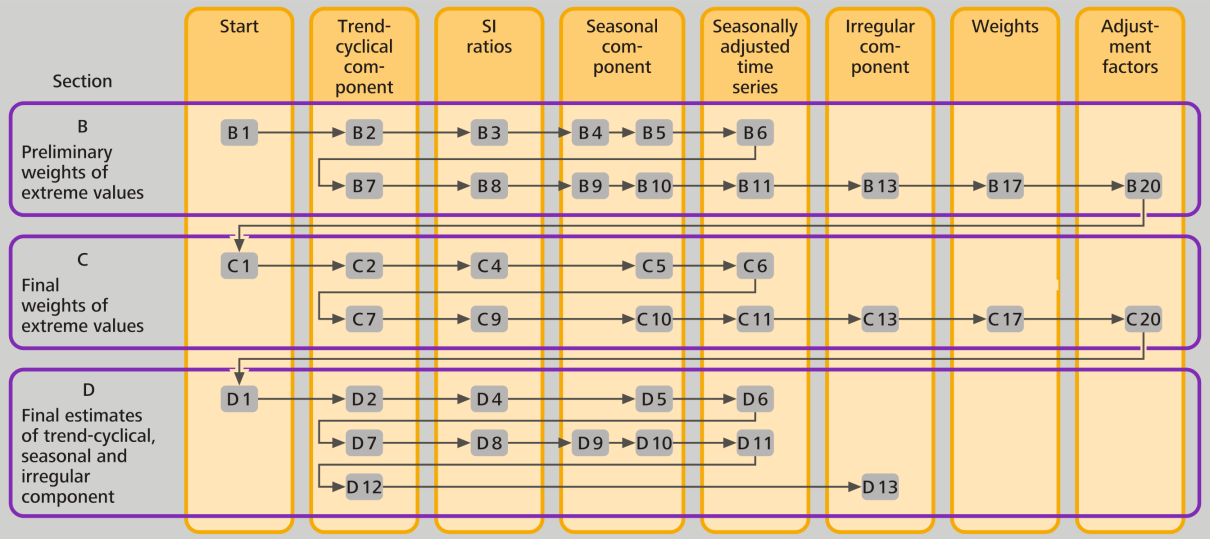


Figure 1: Basic workflow of the classical X-11 method as implemented in JDemetra+. Labels in grey boxes refer to the names of the X-11 output tables.

with $k \in \{1, 3, 5, 9, 15\}$, or with a stable seasonal filter giving the average seasonal-irregular component for each period.

4. Remove the estimated seasonal component from the observed time series to obtain an estimate of the seasonally adjusted data.

This fundamental principle is passed through twice in each of the three X-11 sections labelled B, C, and D. Sections B and C mainly target the detection and down-weighting of extremes in the seasonal-irregular component, whereas Section D actually aims to provide the final estimates of the trend-cyclical, seasonal, and irregular components.

As for Step 1, the input series to the first pass in any of these sections is the linearised time series, possibly corrected for prior adjustment factors and/or extreme values. This series is then smoothed with a composite $2 \times \tau$ moving average, which is a symmetric linear filter that has odd length $\tau + 1$ and admits the polynomial representation

$$\mu(L) = (2\tau)^{-1}(1 + L)S_\tau(L)L^{-\tau/2}, \tag{3}$$

where $S_\tau(L) = (1 - L^\tau)(1 - L)^{-1} = 1 + L + \cdots + L^{\tau-1}$ is the seasonal summation operator associated with periodicity τ. It is easily seen from (3) that the filter's inner weights are $1/\tau$ and the end-points weights are $1/(2\tau)$. In the second pass (and for the final trend-cycle estimation in Section D), the input series is the most recent estimate of the seasonally adjusted data, which is then smoothed with a Henderson filter (Henderson, 1916). This symmetric linear filter has been designed to preserve cubic polynomials or, equivalently, to maximise the estimated trend-cycle's smoothness in the sense of minimising the variance of its third-order differences, as discussed in great detail in Kenny and Durbin (1982). The filter can be represented through

$$\mathcal{H}_m(L) = 1 - (1 - L)^2 \left(1 - L^{-1}\right)^2 \mathcal{H}^\star_m(L),$$

where $m \geq 5$ is the odd filter length and $\mathcal{H}^\star_m(L)$ is a symmetric polynomial of L and L^{-1}

of order $(m-5)/2$. For example,

$$\mathcal{H}_9^\star(L) = 0.04072\left(L^2 + L^{-2}\right) + 0.17277\left(L + L^{-1}\right) + 0.32826,$$

see McElroy (2011) for details on the derivation and more examples. Users may specify any odd filter length $m \in \{3, \ldots, 101\}$, bearing in mind that the weights of $\mathcal{H}_3$ are $(0, 1, 0)$, or rely on an automatic selection based upon the so-called I/C ratio, which is essentially a volatility ratio between tentative estimates of the irregular and trend-cyclical components.

Asymmetric boundary filters are constructed according to the method of Musgrave (1964), which has been designed to minimise the mean squared revision error between the symmetric (target) filter and the asymmetric (approximating) surrogate. The underlying assumption, however, are fundamentally different from those of the symmetric case. Whereas Henderson (1916) assumed that the trend-cycle follows a cubic polynomial and the extraction filter reproduces a cubic polynomial, Musgrave (1964) assumed that the trend-cycle evolves linearly near the sample boundaries and the extraction filter reproduces a constant, see also Doherty (2001) for more details.

As for Step 3, users may specify one $3 \times k$ seasonal filter for all periods or different filters for different periods; alternatively, they can opt for a data-driven selection between the 3×3, 3×5, and 3×9 filters based upon the moving seasonality ratio (Lothian, 1978), that is, a volatility ratio between tentative estimates of the irregular and seasonal components.

2.2 Modified method

We are now mainly interested in seasonally adjusting time series recorded at sub-monthly intervals and, hence, need to relax some of the classical X-11 assumptions. Since sub-monthly time series can exhibit multiple coexisting seasonal patterns with potentially fractional periodicities, we conveniently generalise the classical UC model (1) by introducing the following decomposition of the seasonal component:

$$s_t = \sum_{\tau \in \mathbb{S}} s_t^{(\tau)}. \tag{4}$$

Here, $\mathbb{S} = \{\tau_1, \tau_2, \ldots\}$ is a finite set of periodicities obeying $\tau_i \geq 2$ for all $i \in \{1, 2, \ldots\}$, and $\{s_t^{(\tau)}\}$ denotes the seasonal pattern associated with periodicity $\tau \in \mathbb{S}$. It should also be noted that for sub-monthly time series the classical calendar component in (1) typically collapses to a pure holiday component, as trading and working day variations are not present in such data types.

These subtleties of sub-monthly time series prevent the classical pretreatment model (2) and X-11 filtering routines from being generally applicable. Various modifications are therefore required, which we catalogue in the remainder of this section.

Data linearisation The classical pretreatment model (2) is now replaced with a generalisation of a specific version of model (2). This version is the popular Airline model,

shortly labelled as $(011)(011)_\tau$, and its generalisation[1] is given by

$$(1-L)^d \prod_{\tau\in\mathbb{S}} S_\tau(L)\left(y_t - \mathbf{x}_t^\top \boldsymbol{\beta}\right) = (1-\theta L)\prod_{\tau\in\mathbb{S}}(1-\Theta_\tau L^\tau)\,\varepsilon_t, \tag{5}$$

where $d \in \{1,\ldots,1+|\mathbb{S}|\}$. Model (5) will be referred to as the extended, or fractional, Airline model, as its main novelty—apart from the existence of multiple seasonal summation and MA operators—is an underlying first-order Taylor approximation at unity to fractional powers of the lag operator. This approximation has been introduced to handle fractional periodicities in $\mathbb{S}$ and is given by

$$L^\tau \approx (1-\alpha_\tau)L^{\lfloor\tau\rfloor} + \alpha_\tau L^{\lfloor\tau\rfloor+1}, \tag{6}$$

where $\lfloor\tau\rfloor$ is the largest integer not exceeding τ and $\alpha_\tau = \tau - \lfloor\tau\rfloor$ is the fractional remainder of τ. It thus follows immediately from (6) that the seasonal summation operator in (5) becomes $S_\tau(L) = 1 + L + \cdots + L^{\lfloor\tau\rfloor-1} + \alpha_\tau L^{\lfloor\tau\rfloor}$ for fractional periodicities. Accordingly, model (5) will collapse to the classical Airline model when (a) $|\mathbb{S}| = 1$ in (4), (b) the single seasonal pattern has an integer periodicity (since $\alpha_\tau = 0$ in this case), and (c) full nonseasonal differencing, i.e. $d = 2$, is utilised. This will become relevant in Section 3, where we will empirically compare certain parameter estimates obtained from models (2) versus (5) for the classical case $\tau \in \{4, 12\}$.

A detailed exposition of the extended Airline model, including its limitations and a brief discussion about potential alternatives, is given in Webel and Smyk (2024).

UC estimation The modified X-11 method enables the sequential estimation of the seasonal patterns in (4). Although it breathes the spirit of its classical ancestor (Figure 1), the iterative linear filtering operations have undergone some changes that fall into three main categories: trend-cycle estimation, replacement of extremes in the detrended (alias seasonal-irregular) component, and seasonal estimation. We start with the modifications concerning trend-cycle estimation.

- The crude filter (3) considered for preliminary trend-cycle estimation (B2, C2, D2) has been replaced with a generalised composite $2\times\tau$ moving average, whose length is set to the smallest odd integer not smaller than τ. The inner weights of this new filter remain $1/\tau$, but its end-points weights become $1/\tau$ if τ is an odd integer and $(\mathbb{I}\{\lfloor\tau\rfloor \text{ is even}\}+\alpha_\tau)/(2\tau)$ otherwise. Note that this generalisation exactly replicates the classical 2×4 and 2×12 filters.

- The symmetric Henderson filters and their asymmetric Musgrave surrogates for refined and final trend-cycle estimation (B7, C7, D7, D12) have been replaced with broader families of kernel-based trend-cycle filters that encompass these classical filters. These families are constructed within local polynomial regression models (Proietti and Luati, 2008) and reproducing kernel Hilbert spaces (Aronszajn, 1950),

[1] The current JD+ implementation of model (5) allows for an optional "inversion" of the invertible nonseasonal MA factor, $(1-\theta L)$, into a stationary nonseasonal first-order AR factor of the form $(1-\phi L)$ with $|\phi| < 1$. This replacement, however, will not be useful for our empirical analyses and therefore is not discussed any further in this paper.

allowing for a consistent derivation of asymmetric boundary filters within either methodological framework. Technical details about this probably most remarkable enhancement are given in the Appendix.

- Owing to the multitude of possible configurations for kernel-based trend-cycle extraction (B7, C7, D7, D12), there is currently no routine for a data-driven selection of the most appropriate filter given the input series.

We next point out a simplification regarding the built-in correction of extreme values in the seasonal-irregular component. The classical X-11 method utilises a benchmark moving standard deviation of the irregular variation in conjunction with lower and upper tolerance multipliers, called σ-limits, to calculate replacement values (B4, B9, D9), preliminary and final weights (B17, C17), and corresponding adjustment factors (B20, C20) for such extremes. Thereby, the benchmark dispersion is obtained either from 5-year sliding spans[2] (centred around the current position in time) or as a set of period-specific standard deviations.

- The classical replacement procedure is carried out only in Section B of the modified X-11 method, always using the sliding spans approach (B4, B9), followed by the default calculation of both weights and adjustment factors for the detected extremes (B17, B20, C17, C20). In other words, the extreme-value correction (D9) is simply skipped in the final filtering stage.

We finally list the changes with respect to estimating the seasonal component by smoothing the (corrected) seasonal-irregular component.

- Any pair of $3 \times k$ seasonal moving averages can be specified for preliminary (B5, C5, D5) and final (B10, C10, D10) seasonal estimation. This generalises the idea of the classical X-11 default filters, which refer to the $(3 \times 3,\ 3 \times 5)$ combination.

- However, the specification of different seasonal filters for different periods is impossible.

- When τ is fractional, the seasonal-irregular component (B3, B8, C4, C9, D4, D8) admits a ragged-edge matrix representation that prevents any column-wise smoothing. The specified $3 \times k$ seasonal filters are therefore applied to weighted averages of lagged/led seasonal-irregular values, utilising the Taylor approximation (6) for both symmetric and asymmetric filters (see Webel and Smyk, 2024, for details). The resulting seasonal estimates are finally normalised with the aforementioned generalised $2 \times \tau$ moving average.

- There is currently no routine for a data-driven selection of the most appropriate seasonal filter in the final filtering stage (D10), see Webel (2026) for more insights and a discussion of potential remedies.

- There is currently no dedicated treatment of short time series. Disregarding any user specification, the classical X-11 method automatically resorts to the application

[2]If the series under investigation is shorter than five years, then a single benchmark standard deviation is calculated from the seasonal-irregular values actually available.

of stable seasonal filters in all periods whenever the observed time series is shorter than four years. The modified X-11 method, however, simply spits out an error message when the specified seasonal filters are too long for the given sample size.

3 Methodological maturity for monthly data

The conceptual differences between the classical and modified X-11 methods, laid out in the previous section, demonstrate that the modifications rest on both interesting enhancements and surprising simplifications of the classical computing routines. Since the net effect of these changes is not obvious at all, it seems natural to conduct an empirical evaluation of the modified X-11 method against its classical ancestor that will serve as a benchmark. To this end, we consider a real-time macroeconomic data set of a monthly short-term production indicator for Germany. This example has been chosen because each vintage time series in this set not only contains a fair amount of both working day and seasonal variation, but is also fitted reasonably well by the classical Airline model according to standard residual diagnostics. The idea is to seasonally adjust each vintage series with the two X-11 methods under a concurrent revision regime and to assess potential discrepancies between important target signal estimates. We therefore require the corresponding seasonal adjustment settings to be aligned to one another as much as possible, which is why we now need either an exact kernel-based replication or an excellent kernel-based approximation of the classical Henderson and Musgrave trend-cycle filters.

3.1 Real-time data

We consider monthly production of capital goods in Germany. This is an important macroeconomic series since capital goods constitute the largest of the five main industrial groupings defined in Annex II of European Commission (2020) on the basis of the statistical classification of economic activities in the European Union (Eurostat, 2025). Its current share of total industrial production in Germany is 45.5%, which translates into almost 34% of production in the entire manufacturing sector.

The series is calculated as a Laspeyres volume index, whose base year is normally updated every five years. The entire real-time data set consists of the 242 vintage production indices released between December 2005 and January 2026, having base years of 2000, 2005, 2010, 2015, and 2021.[3] The sample spans always begin in January 1991, but their ends increase gradually from October 2005 in the first vintage to November 2025 in the last vintage; accordingly, the sample sizes grow from 178 to 419 monthly observations across the release vintages. Figure 2 shows the production index released in the last vintage, along with an autoregressive estimate[4] of the spectral density of the differenced logged data. The time series plot highlights not only the long-term trending nature of the index, but also the devastating medium-term effects of the world economic crisis in 2008/2009 and of the COVID-19 pandemic outbreak in March 2020. The estimated spectral density exhibits a local peak at each of the six seasonal frequencies and,

[3]The regular base year update from 2015 to 2020 has been suspended due to the heavy impact of the COVID-19 pandemic on the series.

[4]The model order of $p = 30$ is inherited from the spectral diagnostics settings that apply to monthly time series in the X-12-ARIMA seasonal adjustment program (Soukup and Findley, 1999).

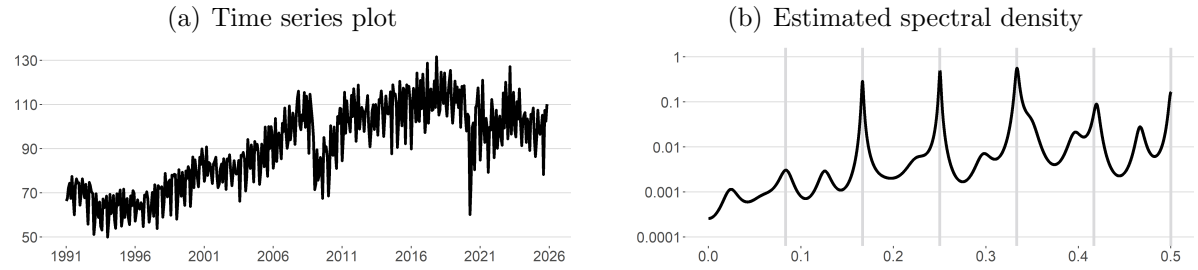


Figure 2: Monthly production of capital goods in Germany. Panel (a) shows the vintage index released in January 2026 (2021 = 100). Panel (b) shows the AR(30) estimate for the spectral density of the differenced logged index (in decibels, abscissa in units of cycles per time). Grey verticals mark the six seasonal frequencies.

hence, provides compelling evidence for the seasonal nature of the series. Furthermore, the right-skewed shape of the local peak at the fourth seasonal frequency is indicative of non-ignorable trading/working day variation.

3.2 Seasonal adjustment settings

We now describe the configuration of the classical and modified X-11 seasonal adjustments. According to our intended concurrent revision policy, each automatic detection or identification routine is re-evaluated for each vintage series; likewise, the parameters of the two Airline pretreatment models are re-estimated from each vintage index.

Data linearisation The additive UC model (1) is obtained after applying the log transformation. The monthly Airline model is obtained from specifying the $(011)(011)_{12}$ variant of model (2) for the classical X-11 method and from setting $\mathbb{S} = \{12\}$ and $d = 2$ in the generalisation (5) for the modified X-11 method. In either case, the monthly numbers of working days (WD) in January through November and in December are added in centred form as two exogenous regression variables, taking into account partial working days due to regional holidays. In addition, additive outliers (AO) and level shifts (LS) are automatically detected, using sample size adjusted 0.01-level critical t-values according to the U.S. Census Bureau's modification to the asymptotic formula derived in Ljung (1993). No back- and forecasts for the unadjusted data are generated from the pretreatment models.

Classical X-11 method The Henderson trend-cycle filter is selected automatically based upon the value of the I/C ratio, so that essentially a choice is being made between the 9-term, 13-term, and 23-term filters. Similarly, the $3 \times k$ seasonal moving average is automatically chosen according to the moving seasonality ratio, so that the list of candidate filters reduces to the 3×3, 3×5, and 3×9 moving averages. This selection, however, then needs to be specified explicitly in the program to be applied throughout all stages of preliminary and final seasonal estimation (B5, B10, C5, C10, D5, D10). Otherwise, the chosen filter would be applied only in the last stage (D10) alongside the X-11 default filters in all preceding stages, which would create an irreproducible combination for the modified X-11 method.

Regarding the automatic detection and correction of extremes in the seasonal-irregular component, we distinguish between four scenarios with respect to the two driving forces, that is, the σ-limits and the way the benchmark moving standard deviation of the irregular variation is obtained:

- *Scenario 1*: σ-limits $= (1.5, 2.5)$ and standard deviations from 5-year sliding spans,
- *Scenario 2*: σ-limits $= (1.5, 2.5)$ and month-specific standard deviations,
- *Scenario 3*: σ-limits $= (2.0, 3.0)$ and standard deviations from 5-year sliding spans,
- *Scenario 4*: σ-limits $= (2.0, 3.0)$ and month-specific standard deviations.

Scenarios 1 and *2* thus bear a higher a priori sensitivity towards detection of extremes, whereas *Scenarios 3* and *4* allow for more generosity in this regard. Also, the settings of *Scenarios 1* and *3* can be replicated in the modified X-11 method, whereas those of *Scenarios 2* and *4* cannot. Consequently, these scenarios will enable us to evaluate important target signal estimates of the modified X-11 method under various levels of stress owing to the missing extreme-value correction in the final filtering stage.

Modified X-11 method We assess both local polynomial regression filters (LPRF) and reproducing kernel Hilbert spaces (RKHS) for kernel-based trend-cycle estimation. The details and examples given in the Appendix suggest that for the relatively short bandwidths required here the exact Henderson and biweight kernels provide the best replications of the classical Henderson and Musgrave filters within either framework, in line with earlier statements made in Proietti and Luati (2008) and Dagum and Bianconcini (2008). We thus restrict our attention to those two kernels here; asymmetric filters are obtained under the linear-constant boundary assumption in the LPRF approach and through optimal bandwidth selection for boundary kernels via the frequency response criterion (17) under a generic random walk assumption in the RKHS approach.

The hard-coded $3 \times k$ seasonal moving average from the classical X-11 method is adopted for both preliminary and final seasonal estimation. As for the detection of extreme seasonal-irregular values, the σ-limits are dictated by *Scenarios 1* through *4* defined above, keeping in mind that the benchmark irregular standard deviation is always calculated from 5-year sliding spans. To gain further insights into the severeness of the omitted calculation of final replacement values (D9), we additionally take the deviations between the extreme-value corrected linearised series (D1) and the most recent trend-cycle estimate (D7) as an unimplemented proxy correction.

3.3 Similarity measure

Let $\{\hat{S}_t\}$ be the estimate of a target signal from UC model (1). To quantify the similarity between the estimates obtained from two competing methods, we will make use of Theil's U_1 coefficient (Theil, 1958). This normalised inequality measure is given by

$$U_1 = \frac{\left\| \hat{S}_t^{(\mathrm{cl})} - \hat{S}_t^{(\mathrm{mo})} \right\|_2}{\left\| \hat{S}_t^{(\mathrm{cl})} \right\|_2 + \left\| \hat{S}_t^{(\mathrm{mo})} \right\|_2} \in [0, 1], \tag{7}$$

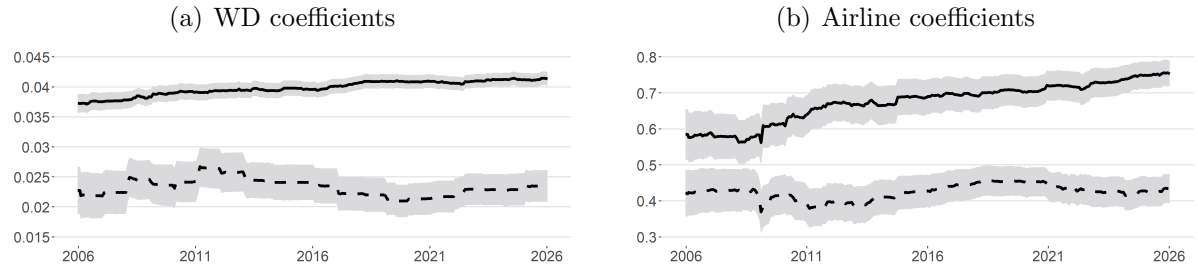


Figure 3: Selected parameter estimates from the $(011)(011)_{12}$ variant of pretreatment model (2) across all release vintages. Panel (a) shows the estimated WD regression coefficients for the January through November (*solid line*) and December (*dashed line*) variables. Panel (b) shows the estimated Airline coefficients $\hat{\theta}$ (*dashed line*) and $\hat{\Theta}_{12}$ (*solid line*). Grey ribbons mark the pointwise ± 1 standard error intervals.

where $||\cdot||_2$ is the vector Euclidean norm and the superscripts in parentheses indicate the X-11 method. Although the U_1 coefficient has some serious drawbacks when evaluating the accuracy of economic forecasts against actual observations (Ahlburg, 1984; Bliemel, 1973; Granger and Newbold, 1973), it provides a "good enough" metric for our empirical in-sample comparison. Values close to zero (one) signal a high (low) degree of similarity between the two estimates.

3.4 Results

Data linearisation The Airline variant of the classical pretreatment model (2) and its generalisation (5) generally produce almost the same results across the considered data vintages. For example, Figure 3 shows the estimated WD regression coefficients and MA parameters obtained from each vintage production index with the classical approach, along with their respective standard errors. The corresponding estimates of the extended Airline model are not displayed, as they are visually indistinguishable from the classical counterparts. Differences between the linearised vintage production series may thus arise only from different outcomes of the automatic outlier detection routines, but, luckily, those tend to be negligible.

To prove this point, Table 1 reports the estimated pretreatment models for the vintage production index released in July 2020. This example has been chosen deliberately, because it showcases the only occurrence of mismatching outlier identifications in the entire real-time data set. More specifically, four outliers are automatically detected in the classical case: a negative level shift in January 2009, related to the world economic crisis, and a stacked (net negative) AO-LS combination in March 2020 followed by a negative additive outlier in April 2020, both related to the COVID-19 pandemic outbreak in Germany. In the extended Airline model, however, only three outliers are automatically detected, as a single negative level shift is identified in place of the stacked AO-LS combination for March 2020 (the other two outliers remain the same). This barely affects the other parameter estimates; the largest absolute difference is observed between the estimated seasonal MA parameters, amounting to 0.0096. When taking all vintage production indices into account, no larger discrepancy has been recorded for any pair of estimated WD regression

Table 1: Estimated pretreatment models for the vintage production index released in July 2020

	Airline variant of model (2)			Extended Airline model (5)		
Parameter	Estimate	S.E.	t-value	Estimate	S.E.	t-value
WD Jan–Nov	0.0408	0.0011	35.8453	0.0412	0.0012	35.2783
WD Dec	0.0213	0.0027	7.9919	0.0213	0.0027	7.7594
LS Jan 2009	−0.1834	0.0213	−8.6172	−0.1832	0.0219	−8.3528
LS Mar 2020	−0.3264	0.0327	−9.9761	−0.2216	0.0248	−8.9266
AO Mar 2020	0.1496	0.0318	4.7050			
AO Apr 2020	−0.2392	0.0284	−8.4113	−0.3138	0.0243	−12.9319
θ	0.4531	0.0405	11.1957	0.4501	0.0420	10.7084
Θ_{12}	0.7036	0.0428	16.4556	0.6940	0.0442	15.6996

and Airline coefficients, including their respective standard errors.

X-11 signal estimates We first note that the automatic filter selection routines of the classical X-11 method pick the 13-term Henderson filter alongside the 3×5 seasonal moving average for each vintage production series, regardless of the scenario for detecting extremes in the detrended data.

Having said that, we proceed to the analysis of potential distortions caused by the missing calculation of replacement values for such extremes during the final seasonal estimation stage in the modified X-11 method. For each vintage production series, we calculate Theil's U_1 coefficient (7) between the classical extreme-value corrected seasonal-irregular component (D9) and two close relatives from the modified X-11 method: the uncorrected seasonal-irregular component (D8) and the unimplemented proxy correction (D1/D7). Figure 4 shows for each of the four extreme-value detection scenarios the kernel densities estimated from the two sets of 242 vintage U_1 coefficients, using LPRF trend-cycle estimation. In general, the Henderson and biweight kernels produce very similar final detrended estimates. Furthermore, the deviations between the classical extreme-value corrected seasonal-irregular component and its uncorrected analogue from the modified X-11 method tend to be small across all data vintages under each scenario, as $U_1 < 0.006$ except for some cases under *Scenario 2*. Unsurprisingly, when comparing the four scenarios, the dissimilarity increases with the sensitivity for detecting extremes; this can be seen from specifying either default rather than higher σ-limits (*Scenario 1* versus *3* and *Scenario 2* versus *4*) or month-specific benchmark irregular standard deviations rather than 5-year sliding spans (*Scenario 2* versus *1* and *Scenario 4* versus *3*). Similar statements can be made when considering the proxy correction in the modified X-11 method, which nevertheless tends to systematically reduce the inequality coefficients ($U_1 < 0.004$ under each scenario); this reduction is slightly larger when default σ-limits are used (*Scenarios 1* and *2*). Therefore, incorporating some form of extreme-value replacement into the final seasonal estimation stage of the modified X-11 method seems beneficial, although the uncorrected estimates and their classical corrected counterparts show no alarming systematic discrepancy. Almost the same conclusion can be drawn when using RKHS instead of LPRF trend-cycle estimation, see Figure 11 in the Appendix.

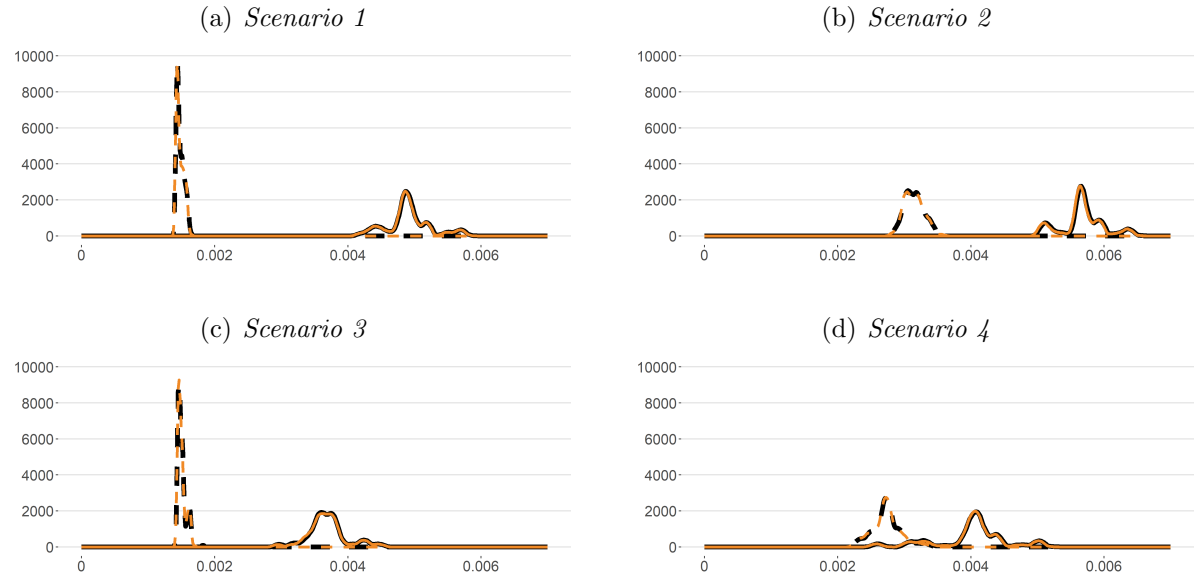


Figure 4: Epanechnikov kernel density estimates for Theil's U_1 coefficient (7) between the extreme-value corrected seasonal-irregular component (D9) from the classical X-11 method and related components from the modified X-11 method. The latter are the unmodified seasonal-irregular component (D8, *solid lines*) and its proxy correction (D1/D7, *dashed lines*); the modified X-11 method utilises local polynomial regression filters with the exact Henderson (*orange lines*) and biweight (*black lines*) kernels.

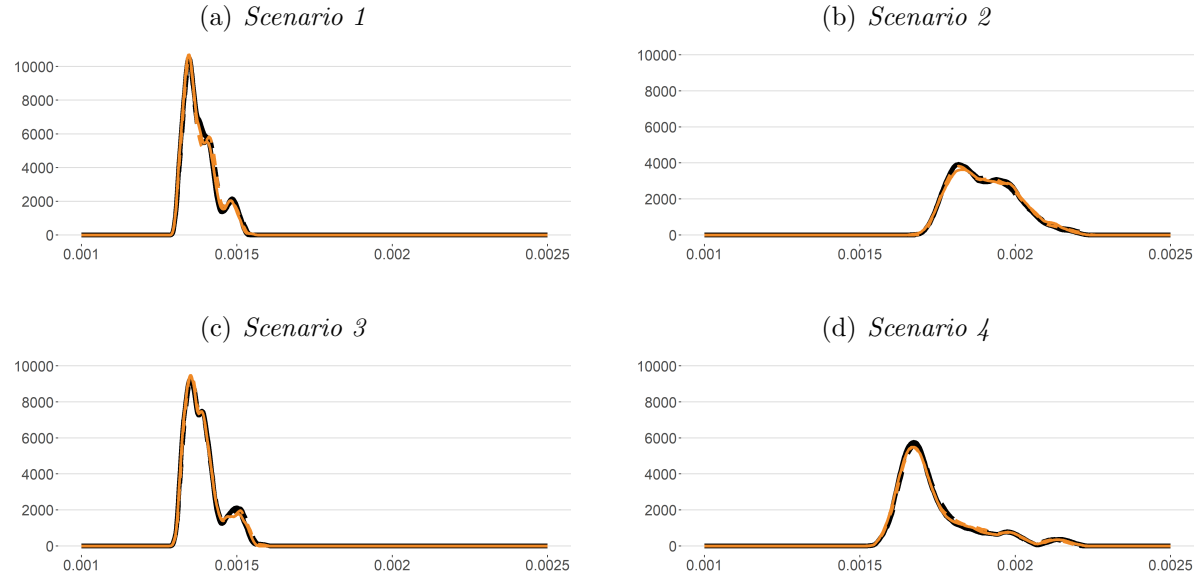


Figure 5: Epanechnikov kernel density estimates for Theil's U_1 coefficient (7) between the seasonally adjusted estimates from the classical and modified X-11 methods, utilising local polynomial regression filters (*solid lines*) and reproducing kernel Hilbert spaces (*dashed lines*) with the exact Henderson (*orange lines*) and biweight (*black lines*) kernels.

Table 2: Month-on-month growth rates of seasonally adjusted production of capital goods in Germany from June through November 2025 (as a percentage, January 2026 release vintage)

Scenario	X-11 method		Kernel	Jun	Jul	Aug	Sep	Oct	Nov
1	Classical			0.74	4.92	−10.18	4.12	1.16	2.55
2				1.06	4.93	−9.07	2.71	1.06	3.49
	Modified	LPRF	Henderson	0.93	4.91	−9.69	3.53	1.15	2.55
			Biweight	0.96	4.91	−9.70	3.55	1.15	2.56
		RKHS	Henderson	0.91	4.89	−9.69	3.54	1.14	2.59
			Biweight	0.96	4.90	−9.68	3.53	1.14	2.59
3	Classical			0.86	5.00	−8.25	1.83	1.13	2.52
4				0.75	4.72	−8.82	2.75	1.13	2.53
	Modified	LPRF	Henderson	0.84	4.99	−8.60	2.21	1.12	2.52
			Biweight	0.84	4.98	−8.56	2.19	1.11	2.52
		RKHS	Henderson	0.85	4.97	−8.58	2.19	1.12	2.63
			Biweight	0.84	4.97	−8.58	2.20	1.12	2.62

Note: Grey cells mark the replacement of extremes in the classical final seasonal-irregular component (D8).

Next, we assess the potential systematic distortions between the seasonally adjusted vintage production indices obtained from the classical and modified X-11 methods. Figure 5 shows the kernel density estimates for their vintage U_1 coefficients (7) under each extreme-value detection scenario. In general, $U_1 < 0.0025$ under each scenario, indicating yet again a high overall similarity between the two signal estimates, regardless of both the kernel-based approach to trend-cycle estimation and the kernel configuration therein. Note also that the estimated kernel densities have almost the same shape under *Scenarios 1* and *3*.

However, when monitoring economic developments in practice, the attention usually shifts from the bird's-eye view to the recent end of the sample span. Table 2 mimics this change in perspective, as it compares the final six month-on-month growth rates of the various seasonally adjusted production indices from the January 2026 release vintage that have been calculated from the two X-11 methods under the different settings employed in this section. In general, each seasonally adjusted estimate experiences volatile zigzag dynamics between June and November 2025, increasing five times during this phase with growth rates ranging broadly between 0.7% in June and 5% in July. This upward tendency is only interrupted by a sharp drop in August, which averages to −9.1% over all seasonally adjusted estimates. It is also seen that the configuration of the kernel-based trend-cycle filter in the modified X-11 method barely affects the growth rates in most months under either choice of σ-limits; those are also in close agreement with the growth rates of the classical X-11 estimates in June, July, October, and November (except for *Scenario 2*).

In contrast, quite different dynamics between the classical and modified X-11 estimates can be observed in August and September, and those seem to be partially triggered by the actual correction of extremes in the classical final seasonal-irregular component. Under

Scenario 1, for example, such extremes have been spotted in July and August, leading to growth rates of -10.2% in August followed by 4.1% in September, whereas the corresponding rates of the modified X-11 estimates are roughly -9.7% and 3.5%, respectively. Differences of similar magnitude have also been recorded under the other extreme-value detection scenarios. The frequent occurrence of such extremes in the months of July and August is a common facet of many German production series and often rationalised through the moving dates of regional school holidays in the summer, which are regularly coordinated by federal state authorities before their official adoption by the Standing Conference of the Ministers of Education and Cultural Affairs. According to harmonised recommendations for sound seasonal adjustment practices in Europe (Eurostat, 2024), such granular holiday-related effects often cannot be estimated reliably from monthly data and, hence, should not be removed from the corresponding official seasonally adjusted figures.

Nevertheless, this cautionary example shows that the seasonally adjusted real-time production indices obtained with the classical and modified X-11 methods—although evolving quite similarly in general over their vintage sample spans—can still display zoomed-in dynamics, especially at the recent end of the sample span that differ to an extent which some practitioners may find unacceptably high. Such discrepancies can typically be traced back to the present rudimentary character of the built-in extreme-value correction in the modified X-11 method, highlighting the need for future improvements into this direction.

4 Empirical performance for sub-monthly data

The previous empirical maturity assessment of the modified X-11 computing routines has exploited the well-known fact that the classical Henderson and Musgrave trend-cycle filters can be exactly replicated within the LPRF framework and closely approximated within the RKHS framework, using the exact Henderson and biweight kernels, respectively, under appropriate boundary conditions. Our attention now shifts from monthly to sub-monthly time series and, hence, from kernel-based trend-cycle filters with relatively short bandwidths to those with longer bandwidths. This brings up two additional questions. The first one concerns the choice of an appropriate kernel. Recalling the basic X-11 workflow diagram (Figure 1), the configuration of the trend-cycle filter may set free a chain reaction that can heavily affect the quality of the final seasonal and seasonally adjusted estimates. We thus ask if there are kernels, which—although they produced a rather poor approximation to the classical 13-term Henderson filter according to Table 5 in the Appendix—can outperform the exact Henderson and biweight kernels with longer bandwidths in terms of seasonal adjustment adequacy. In a way, this part of our analysis extends a previous discussion centred around the triweight kernel (Loader, 1999). The second question concerns the derivation of asymmetric boundary filters; it is primarily motivated by the fact that the classical Musgrave assumption, according to which the trend-cycle admits a local linear representation near the sample boundaries, may not hold for sub-monthly data. We thus ask if there are alternative assumptions, or criteria, that enable the construction of more appropriate boundary filters in the case of longer bandwidths.

Overall, the subsequent study is designed to treat the kernel-based Henderson and

biweight trend-cycle filters under the classical Musgrave assumption (and the preservation of cubic polynomials) as a benchmark and to evaluate the potential added value from using other kernels and/or boundary conditions in concurrent modified X-11 seasonal adjustments of daily and weekly real-time economic time series. Added value will generally be associated with less revisions in the automatic selection of seasonal filters over time, lower real-time revisions in concurrent seasonally adjusted estimates, and especially a lower degree of systematic seasonal adjustment inadequacy. The last criterion will primarily be judged by the sign and size of remaining sample first-order seasonal autocorrelations, say $\hat{\rho}_\tau$, in the differenced logged seasonally adjusted data. More specifically, we will estimate $\hat{\rho}_\tau$ from each seasonally adjusted vintage time series in the real-time data set and calculate a kernel density estimate from the obtained values. Systematic seasonal adjustment inadequacy is then signalled if this kernel density estimate has most of its mass in the range $[\epsilon, 1]$ (under-adjustment) or in the range $[-1, -\epsilon]$ (over-adjustment) for some $\epsilon > 0$; this threshold will be determined as the average Bartlett approximation to the large-lag standard error of $\hat{\rho}_\tau$, where the average is taken over all vintages.

4.1 Weekly Google searches for unemployment

Real-time data This Google trends series covers weekly search activity from Sunday through Saturday for the term "Arbeitslosigkeit", that is, the German translation of unemployment. Our real-time data set collects the 208 vintage series released between W01 2022 and W52 2025. These series start in W02 2004, but their ends increase from W52 2021 through W51 2025; accordingly, the sample sizes grow from 939 to 1,146 weekly observations across the data set. Note, however, that Google's download restrictions with regards to sample size have enforced an artificial construction of these long vintage series from non-overlapping 5-year sequences, see Webel (2025) for details.

Figure 6 shows the Google searches released in the last vintage along with an autoregressive estimate of the spectral density for the differenced logged series. The time series plot reveals that in general weekly search activity for unemployment has declines steadily between 2004 and 2008, experienced a longer tent-like evolution in the wake of the world economic crises in 2008/2009, and then plateaus around 140 despite two short-lived outbursts, one immediately after the COVID-19 pandemic outbreak in March 2020 and one

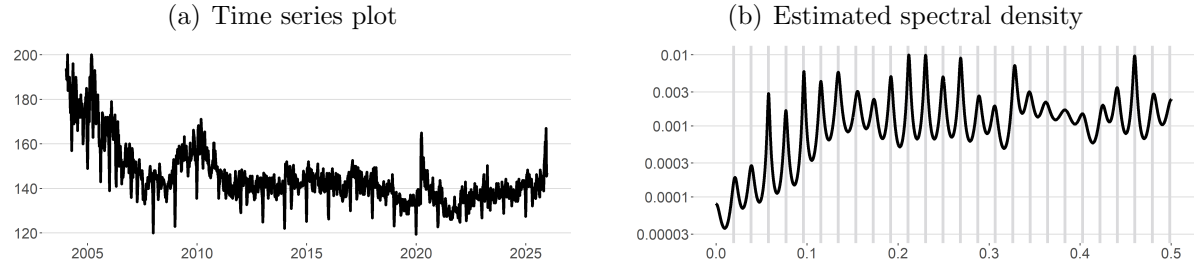


Figure 6: Weekly Google searches for unemployment. Panel (a) shows the vintage series released in W52 2025. Panel (b) shows the AR(60) estimate for the spectral density of the differenced logged series (in decibels, abscissa in units of cycles per time). Grey verticals mark the 26 week-of-the-year frequencies.

in November 2025. The estimated spectral density provides compelling evidence for the presence of seasonal dynamics, as it displays a local peak at each of the 26 week-of-the-year (WOY) frequencies, given by $\omega_j = 2\pi j/52.18$ for $j \in \{1, \ldots, 26\}$.

Seasonal adjustment settings Each vintage Google series is logged to obtain the additive UC model (1). Data linearisation utilises the extended Airline model (5) with $\mathbb{S} = \{52.18\}$ and $d = 2$ to remove deterministic holiday variation related to Carnival, Good Friday, Easter Monday, Pentecost, Corpus Christi, Christmas, and New Year. This step also includes the automatic detection of additive outliers and level shifts based upon sample size adjusted 0.01-level critical t-values. No back- and forecasts are generated from model (5).

Preliminary and final estimation of the WOY pattern in (4) is carried out with the $3\times k$ seasonal moving average that has been automatically selected by a redesigned moving seasonality ratio under the quartiles intersection rule (Webel, 2026). This ratio is calculated from the proxy correction of the final seasonal-irregular component (D1/D7), after using the default σ-limits of $(1.5, 2.5)$ in the preceding extreme-value correction steps. All kernels and boundary conditions available in the LPRF and RKHS frameworks will be considered for parametric trend-cycle estimation with 55-term filters. As detailed in the Appendix, there are six ways to derive asymmetric LPRF filters: the direct asymmetric filters (12), the cut-and-normalise approach (13), and the so-called constant-constant, cubic-quadratic, linear-constant, and quadratic-linear cases, which basically refer to the different polynomial trend degrees to be preserved by the boundary filters. Asymmetric RKHS filters are constructed through four spectral criteria for the optimal bandwidth selection of boundary kernels: the frequency response criterion (17), the accuracy criterion (19), the timeliness criterion (20), and the smoothness criterion (21). In essence, the rationale of these criteria is to translate Musgrave's minimisation problem from the time domain into the frequency domain, where either the mean squared filter revision error or certain components thereof are minimised over appropriate frequency bands. The accuracy and timeliness criteria, for example, utilise the filter's pass-band, which is generally given by $[0, \underline{\omega}]$ for some $\underline{\omega} > 0$ and defined here through $\underline{\omega} = 2\pi/52.18$. For the sake of completeness, we finally note that applying the smoothness criterion currently throws an error message when the filter length exceeds 23 terms; for that reason, we resort to setting these local bandwidths to $(55 + 1)/2 = 28$, in line with related studies (Dagum and Bianconcini, 2008, 2013).

Data-driven selection of seasonal filters When estimating the trend-cycle with one of the benchmark filters, the 3×9 seasonal filter is automatically selected for most vintage Google searches. Occasional exceptions include some series released in early 2022, for which the longer 3×15 filter is automatically picked, as well as some series released during the first half of 2024, for which the shorter 3×5 filter is chosen. This overall picture does not change dramatically when other kernel configurations are considered. In the LPRF framework, for example, switching to another kernel while retaining Musgrave's boundary assumption results in a different seasonal filter selection for at most 13 out of the 208 vintage Google searches; this worst case is observed for the uniform kernel, while the number of different filter choices lies between 1 and 8 for the other kernels. Changing the derivation of asymmetric boundary filters has an even lesser effect, as it results in

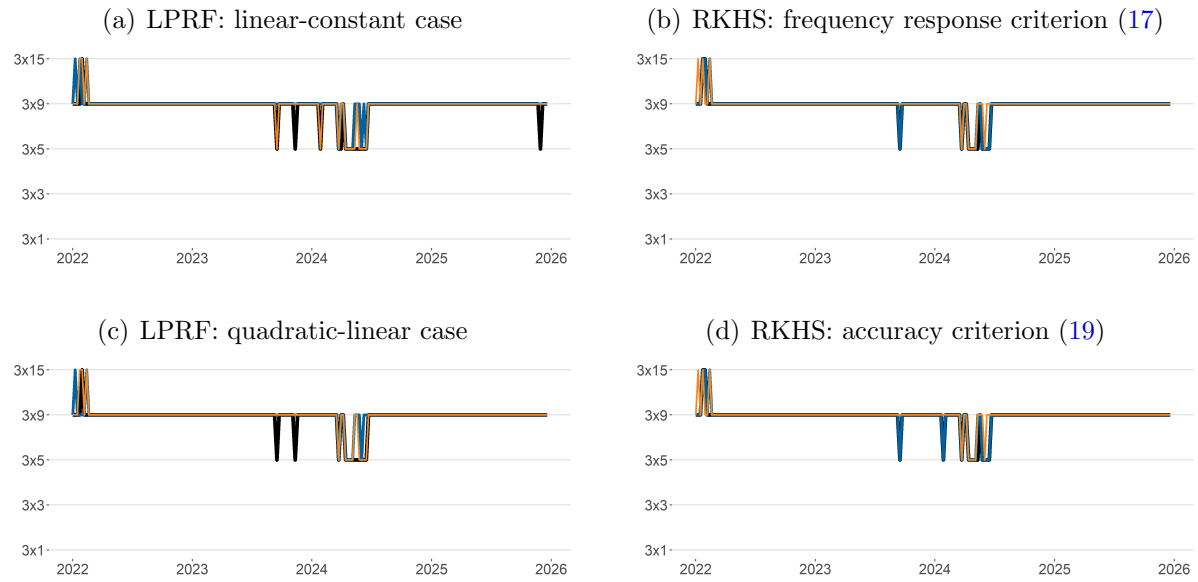


Figure 7: Automatic selection of $3 \times k$ seasonal filters for extracting the week-of-the-year pattern from the Google searches released in the W01 2022 through W52 2025 data vintages. Panels (a) and (c) show the selected filters when using trend-cycle estimation based upon local polynomial regression filters with the Henderson (*black lines*), uniform (*blue lines*), and Gaussian (*orange lines*) kernels. Panels (b) and (d) show the selected filters when using trend-cycle estimation based upon reproducing kernel Hilbert spaces with the biweight (*black lines*), Epanechnikov (*blue lines*), and uniform (*orange lines*) kernels, where bandwidth selection for boundary kernels assumes a random walk in the specified optimality criteria.

a maximum of 5 different filter selections, taking all kernels in the LPRF and RKHS frameworks into account. Actually, that is no surprise given that the redesigned moving seasonality ratio operates on complete years. Figure 7 shows some examples.

Seasonal adjustment adequacy We now assess the sample lag-52 autocorrelations of the differenced logged seasonally adjusted vintage Google searches. This evaluation is mainly motivated by the minor symptoms of over-adjustment that have previously been documented for the W01 2022 through W01 2024 release vintages (Webel, 2025). In fact, this earlier revision study focused on LPRF trend-cycle estimation with the Henderson kernel under the linear-constant boundary assumption in combination with a user-specified 3×5 seasonal filter and found an unimodal estimated kernel density for $\hat{\rho}_{52}$ with support $[-0.15, -0.05]$ and $\epsilon = 0.0363$.

Figure 8 reconstructs this past scenario in Panel (a), showing that the application of the automatically selected seasonal filters indeed mitigates the aforementioned over-adjustment issue, as the support of the kernel density estimate now shifts to $[-0.1, 0.03]$. It is also seen that switching from LPRF trend-cycle estimation to the RKHS methodology with the biweight kernel and optimal bandwidth selection for boundary kernels via the frequency response criterion (17) has virtually no effect on the estimated kernel density. This is also true for the other LPRF and RKHS kernel configurations. However, when adding the sample lag-52 autocorrelations from the seasonally adjusted vintage Google

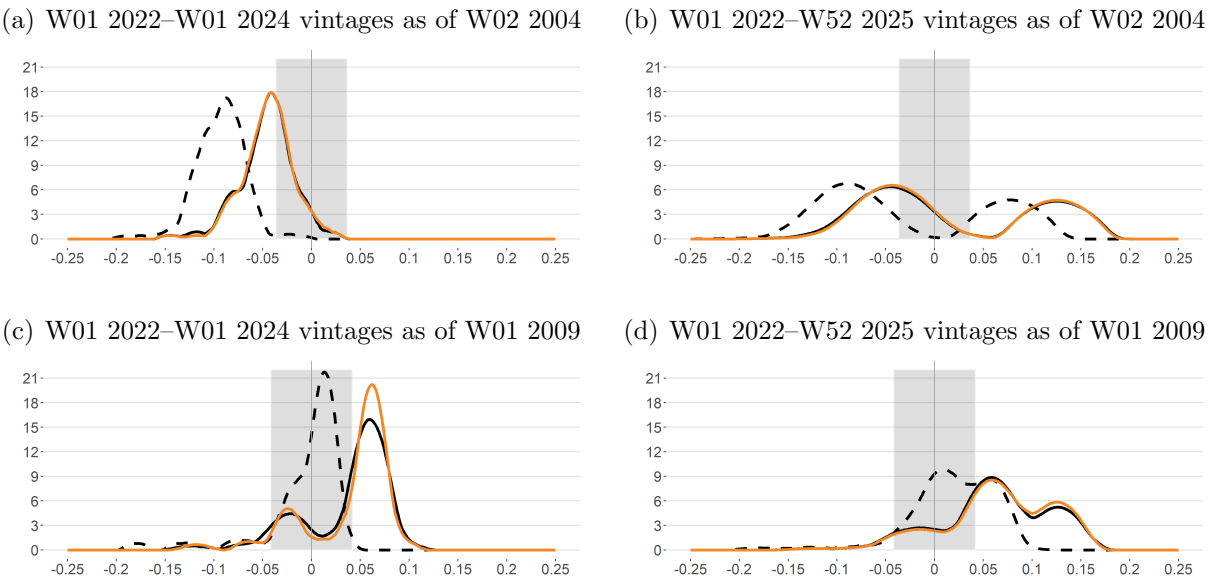


Figure 8: Epanechnikov kernel density estimates for $\hat{\rho}_{52}$ obtained from the differenced logged seasonally adjusted vintage Google searches. Kernel-based trend-cycle estimation is carried out (1) with the Henderson kernel under the linear-constant boundary assumption in the LPRF approach in conjunction with X-11 default seasonal filters (*dashed black lines*) and automatically selected seasonal filters (*solid black lines*), and (2) with the biweight kernel under the frequency response criterion (17) in the RKHS approach in conjunction with automatically selected seasonal filters (*orange lines*). Shaded areas mark ±1 average Bartlett approximation to the large-lag standard error of $\hat{\rho}_{52}$.

searches released after W01 2024, Panel (b) reveals the emergence of an additional under-adjustment issue. More precisely, the estimated kernel densities become noticeably flatter and bimodal, peaking around -0.1 and 0.075 when using the X-11 default seasonal filters and around -0.05 and 0.125 when using the automatically selected seasonal filters. A detailed inspection shows that the large positive values of $\hat{\rho}_{52}$ are exclusively recorded for the longer vintage Google searches released from W26 2024 onwards. Interestingly, this week marks the end of the weekly updates of the Google searches within the first 5-year sub-span, that is, the phase of rapid decline in search activity between W02 2004 and W52 2008 according to Figure 6.

For that reason, we now disregard the first 5-year sub-span and repeat the entire quality assessment with the shortened and less trending vintage Google searches starting in W01 2009. Panel (c) of Figure 8 demonstrates that in this case the systematic over-adjustment issue reported for the 3×5 seasonal filter in Webel (2025) disappears, as a large portion of the support of the estimated kernel density for $\hat{\rho}_{52}$ is now covered by the interval $[-\epsilon, \epsilon]$ with $\epsilon = 0.0416$. When relying on automatic filter selection, however, the occasional choice of the 3×15 seasonal filter for some earlier vintage Google searches needs to be overwritten with the 3×9 seasonal filter, owing to the shorter sample sizes. It is also noted that the configuration of the LPRF and RKHS trend-cycle filters has now a slightly greater impact on the automatic filter selection, which in general meanders much more erratically between the 3×5 and 3×9 filters over time. In particular, Figure 12 in the

Appendix shows that the former is selected much more frequently for the vintage Google searches released after W26 2023, but, overall, the latter still remains the filter of choice in the majority of cases. Returning to Panel (c) of Figure 8, the resulting kernel density estimates for $\hat{\rho}_{52}$ are skewed bimodal with a local peak near -0.03 and a global peak near 0.06, revealing mild symptoms of under-adjustment. When considering all vintages, Panel (d) shows that these symptoms become even stronger, as each estimated kernel density displays a flatter shape with a support stretching out to 0.1 when using the X-11 default seasonal filters and to 0.18 when using the automatically selected seasonal filters.

Overall, the reported consistent seasonal adjustment inadequacies, expressed through systematic non-zero sample lag-52 autocorrelations in the seasonally adjusted vintage Google searches, are more a concern of selecting appropriate seasonal filters. The configuration of the kernel-based trend-cycle filter seems to have little to no effect on this particular quality metric when considering the entire vintage sample spans. However, cutting just the first five years from our long real-time data set has already caused significant changes in both the location and the curvature of the kernel density estimates for $\hat{\rho}_{52}$. What is more, the settings for kernel-based trend-cycle estimation have gained relevance for these shortened vintage series, which is also underlined in Figure 13 in the Appendix. All things considered, specifying adequate seasonal adjustments of weekly Google searches is difficult, as this task heavily depends upon the considered vintage series and their sample spans. This is mainly due to the inherent unstable seasonality stemming from the fact that, owing to the lack of publicly available information regarding Google's data compilation policy, almost the entire data history is revised with each new weekly release, see also Cebrián and Domenech (2023, 2024) and Fenga (2020) for recent expressions of similar quality concerns. Practitioners could thus be tempted to run separate seasonal adjustments over non-overlapping data segments once and then to regularly update only the seasonally adjusted estimates in the last segment.

4.2 Daily realised electricity consumption

Real-time data This consumption series covers electricity supplied to the network for the general supply, excluding electricity supplied to the railroad network and to internal industrial and closed distribution networks as well as electricity consumed by the producers. Our real-time data set consists of weekly downloads of the daily time series compiled by the Federal Network Agency, that is, the original data provider. It contains the 208 vintage consumption series released between W01 2022 and W52 2025; these series jointly start on 1 January 2015 and end on 30 December 2021 in the first release vintage through 21 December 2025 in the last release vintage, with sample sizes gradually increasing from 2,556 to 4,008 daily observations. The measurement unit is gigawatt hours (GWh).

Figure 9 highlights the fact the raw data display two superimposed layers of seasonal dynamics. The first layer, exemplified in Panel (a), is formed by repetitive U-shaped infra-yearly movements, resulting from most consumers' unsurprising habit of requiring more electricity in the winter than in the summer, in combination with deep V-shaped troughs around the turn of the years. These persistent swings will be called the day-of-the-year (DOY) pattern, which, however, undergoes two noteworthy changes over time. The first one is the temporary yet atypically sudden decline in the spring of 2020, which has been caused by the first nationwide COVID-19 lockdown with effect from 22 March to

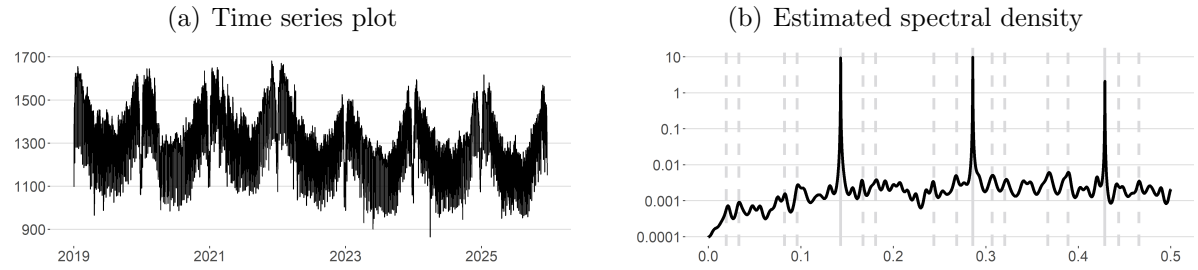


Figure 9: Daily realised electricity consumption. Panel (a) shows the vintage series released in W52 2025 as of 1 January 2019. Panel (b) shows the AR(120) estimate for the spectral density of the differenced logged series (in decibels, abscissa in units of cycles per time). Grey verticals mark the day-of-the-week frequencies (*solid lines*) and selected day-of-the-year harmonics (*dashed lines*).

4 May 2020. The second change in the DOY dynamics is a structural decrease by about 150–200 GWh in peak consumption during the winter as of 2022. This drop has been stimulated by a nationwide energy saving campaign owing to reduced gas imports from Russia, the largest gas exporter to Germany in 2021 (52% of total gas imports) and still the second largest in 2022 (22%) after Norway (33%).

The estimated spectral density, shown in Panel (b), reveals the second seasonal layer of the data that is difficult to spot in the time series plot in Panel (a). This function displays outstanding peaks at 1/7, 2/7, and 3/7, which reflect cyclical phenomena in daily data that occur once, twice, and thrice a week; those dominant recurring dynamics will therefore be referred to as the day-of-the-week (DOW) pattern. A closer look at the raw data uncovers that daily electricity consumption is typically higher from Monday through Friday and significantly lower on Saturday and especially Sunday, mirroring primarily the different amounts of energy demanded from institutional versus private consumers.

Seasonal adjustment settings Each vintage electricity consumption series is considered in logged form. Data precleaning utilises the extended Airline model (5) with $\mathbb{S} = \{7, 365.2425\}$ and $d = 2$. This step includes the automatic detection of additive outliers and level shifts based upon length-adjusted 0.01-level critical t-values and the permanent removal of deterministic calendar variation related to a total of 17 standard national and regional holidays in Germany; the beginning and end of daylight saving time is also taken into account, see Webel (2025) for details. Again, no back- and forecasts of the raw data are generated from model (5).

The $3 \times k$ seasonal moving average for both preliminary and final estimation of the DOW pattern in (4) is automatically picked according to a redesigned moving seasonality ratio under the quartiles intersection rule (Webel, 2026). As in the Google example, this ratio is calculated from the proxy correction of the final seasonal-irregular component (D1/D7), after using the default σ-limits of $(1.5, 2.5)$ in the preceding extreme-value correction steps. The DOY pattern in (4), however, is always estimated with the X-11 default filters due to sample size restrictions. As for kernel-based trend-cycle estimation, the filter length is generally set to the smallest odd integer larger than the periodicity of the seasonal pattern to be extracted; more specifically, 9-term trend-cycle filters are ap-

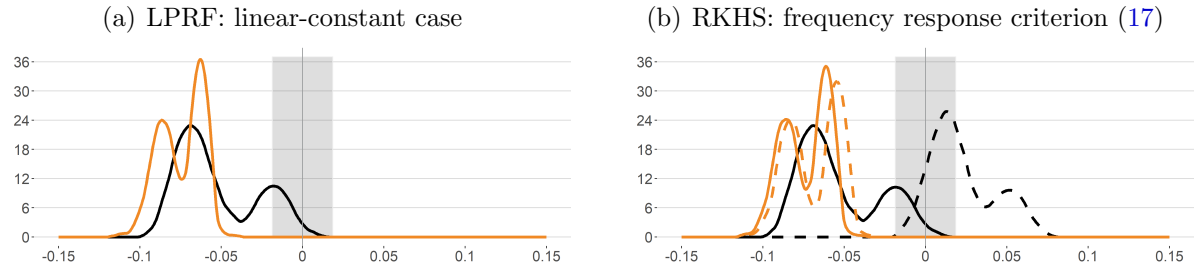


Figure 10: Epanechnikov kernel density estimates for $\hat{\rho}_7$ (*black lines*) and $\hat{\rho}_{365}$ (*orange lines*) obtained from the differenced logged seasonally adjusted vintage consumption series. Kernel-based trend-cycle estimation is carried out with the Henderson kernel in Panel (a) and with the biweight (*solid lines*) and uniform (*dashed lines*) kernels in Panel (b). Shaded areas mark ± 1 average Bartlett approximation to the large-lag standard error of $\hat{\rho}_{365}$.

plied when extracting the DOW pattern, whereas 367-term trend-cycle filters are applied during the estimation of the DOY pattern. We again consider all kernel configurations available in the LPRF and RKHS frameworks in either estimation step, see the overview in the previous section. The filter's pass-band, required when determining the optimal bandwidths for asymmetric RKHS boundary kernels through the accuracy criterion (19) and the timeliness criterion (20), is set to $\underline{\omega} = 2\pi/\tau$, where $\tau \in \mathbb{S}$. Following Dagum and Bianconcini (2008, 2013), we additionally consider fixing these local bandwidths to $(9+1)/2 = 5$ for DOW estimation and to $(367+1)/2 = 184$ for DOY estimation.

Data-driven selection of DOW seasonal filters In contrast to the Google example, the configuration of the LPRF and RKHS trend-cycle filters barely affects the automatic selection of the DOW extraction filter, as the 3×5 seasonal filter is almost always suggested for all vintage consumption series. The only exception occurs for the RKHS methodology when utilising the uniform kernel; in this particular case, the longer 3×9 seasonal moving average is automatically picked, regardless of the specified boundary condition.

Seasonal adjustment adequacy We now briefly evaluate the sample lag-7 and lag-365 autocorrelations of the differenced logged seasonally adjusted vintage consumption series. Brevity is sufficient here, since the estimated kernel densities for both $\hat{\rho}_7$ and $\hat{\rho}_{365}$ barely differ between the various trend-cycle filter configurations, mainly as a consequence of the previous result. Figure 10 shows two typical examples, highlighting their bimodal shape for either lag over the corresponding supports $[-0.1, 0]$ for the lag-7 autocorrelations and $[-0.1, -0.05]$ for the lag-365 autocorrelations. Given that $\epsilon = 0.0186$, these findings point towards a minor systematic over-adjustment issue surfacing at both lags. Unsurprisingly, the only noteworthy exception from this common picture occurs when the DOW pattern is consistently extracted with the 3×9 seasonal filter from each vintage consumption series. As exemplified in Panel (b), the support of the kernel density estimate for $\hat{\rho}_7$ shifts to $[-0.025, 0.075]$ in this case and, hence, indicates that an undesired amount of DOW dynamics has remained in some seasonally adjusted data. Note that Webel (2025) arrived at almost the same conclusion when running LPRF trend-cycle estimation based upon the exact Henderson kernel in conjunction with a hard-coded 3×9 seasonal filter

for estimating the DOW pattern.

Revisions in seasonally adjusted estimates We finally study the revisions in the seasonally adjusted vintage consumption series. However, the previous results and our intended focus on kernel-based trend-cycle extraction filters with longer bandwidths motivate a minor design change with respect to the DOW estimation step. Instead of considering all available kernel configurations, we now specify the exact Henderson kernel with the linear-constant boundary assumption in the LPRF case and the biweight kernel with boundary variants being determined through the frequency response criterion (17) under the random walk assumption in the RKHS case. The resulting trend-cycle filters have already been shown to perform particularly well for shorter bandwidths, see, for instance, the detailed discussion in the Appendix as well as those given in Proietti and Luati (2008) and Dagum and Bianconcini (2008).

We introduce some additional notations before presenting the results. Let $\mathbf{v}_i$ denote the vintage of the raw series $\{y_t\}$ released in the i-th period of some finite span $\{1, \dots, T\}$ and $\{\hat{S}_{t|\mathbf{v}_i}\}$ be an estimated signal of interest obtained from the data stored in $\mathbf{v}_i$. The concurrent and final signal estimates are then given as $\{\hat{S}_{t|\mathbf{v}_{i(t)}}\}$ and $\{\hat{S}_{t|\mathbf{v}_T}\}$, respectively, where $i(t)$ is a function of time that picks the period of the inaugural release of y_t. Revisions in later signal estimates can now be expressed as the percentage change experienced in the level of the concurrent estimates (LCE); the corresponding final and lag-k LCE revisions are defined as the sequences $\{r_t\}$ and $\{r_t(k)\}$ with

$$r_t = 100 \times \frac{\hat{S}_{t|\mathbf{v}_T} - \hat{S}_{t|\mathbf{v}_{i(t)}}}{\hat{S}_{t|\mathbf{v}_{i(t)}}} \quad \text{and} \quad r_t(k) = 100 \times \frac{\hat{S}_{t|\mathbf{v}_{i(t)+k}} - \hat{S}_{t|\mathbf{v}_{i(t)}}}{\hat{S}_{t|\mathbf{v}_{i(t)}}}, \tag{8}$$

respectively. An alternative approach is to assess the percentage points changes in the period-on-period growth rates (PGR) between later and concurrent signal estimates; the corresponding final and lag-k PGR revisions are given by the sequences $\{r_t^{\%}\}$ and $\{r_t^{\%}(k)\}$ with

$$r_t^{\%} = \Delta^{\%}\hat{S}_{t|\mathbf{v}_T} - \Delta^{\%}\hat{S}_{t|\mathbf{v}_{i(t)}} \quad \text{and} \quad r_t^{\%}(k) = \Delta^{\%}\hat{S}_{t|\mathbf{v}_{i(t)+k}} - \Delta^{\%}\hat{S}_{t|\mathbf{v}_{i(t)}}, \tag{9}$$

where

$$\Delta^{\%}\hat{S}_{t|\mathbf{v}_i} = 100 \times \frac{\hat{S}_{t|\mathbf{v}_i} - \hat{S}_{t-1|\mathbf{v}_i}}{\hat{S}_{t-1|\mathbf{v}_i}}.$$

Final revisions concern the relatively remote past; their mean and volatility are typically associated with the reliability of concurrent estimates in the sense of measuring systematic bias from and dispersion around final estimates. Lag-k revisions complementary concern the more recent past and, hence, are typically more important for data users, who tend to be interested predominantly in the case $k = 1$.

We calculate the final and lag-1 revision sequences defined in (8) and (9) from the seasonal adjustments of the vintage consumption series released between W01 2022 and W52 2024, with final estimates being obtained from the W52 2025 release vintage. Table 3 reports the mean revision, the mean absolute revision, and the standard deviation of the revisions for each of these sequences under each LPRF trend-cycle filter configuration; Table 4 does the same for the various RKHS trend-cycle filters. Overall, the resulting revision profiles are very similar, so that it is impossible to identify a particular LPRF or

Table 3: Revisions in seasonally adjusted daily electricity consumption under LPRF trend-cycle estimation

		LCE revisions (8)						PGR revisions (9)					
		Final revisions $\{r_t\}$			Lag-1 revisions $\{r_t(1)\}$			Final revisions $\{r_t^{\%}\}$			Lag-1 revisions $\{r_t^{\%}(1)\}$		
Kernel	Boundary condition	MR	MAR	SD	MR	MAR	SD	MR	MAR	SD	MR	MAR	SD
Biweight	LC	−0.5295	2.4847	2.9639	−0.0953	0.4417	0.7890	−0.0116	1.1157	1.5567	−0.0046	0.4809	0.7505
	QL	−0.5449	2.6494	3.1278	−0.0812	0.4510	0.8028	−0.0110	1.1063	1.5452	−0.0042	0.4839	0.7524
	DA via (12)	−0.4785	2.5721	3.0604	−0.0671	0.4970	0.8349	−0.0087	1.0894	1.5241	−0.0020	0.4838	0.7767
	CN via (13)	−0.5153	2.4979	2.9777	−0.0972	0.4285	0.7776	−0.0112	1.1144	1.5599	−0.0042	0.4700	0.7360
Gaussian	LC	−0.5221	2.4693	2.9512	−0.0984	0.4424	0.7892	−0.0115	1.1154	1.5570	−0.0045	0.4792	0.7494
	QL	−0.5418	2.6369	3.1154	−0.0869	0.4575	0.8106	−0.0107	1.1013	1.5439	−0.0040	0.4871	0.7654
	DA via (12)	−0.4794	2.5961	3.0819	−0.0716	0.4945	0.8312	−0.0093	1.0889	1.5262	−0.0027	0.4863	0.7786
	CN via (13)	−0.5037	2.4785	2.9618	−0.1005	0.4334	0.7834	−0.0112	1.1164	1.5615	−0.0042	0.4741	0.7467
Henderson	LC	−0.5361	2.4985	2.9756	−0.0947	0.4400	0.7894	−0.0118	1.1167	1.5602	−0.0047	0.4822	0.7546
	QL	−0.5462	2.6568	3.1349	−0.0772	0.4512	0.8048	−0.0112	1.1053	1.5439	−0.0043	0.4871	0.7575
	DA via (12)	−0.4847	2.5694	3.0554	−0.0720	0.5008	0.8391	−0.0086	1.0880	1.5155	−0.0019	0.4887	0.7812
	CN via (13)	−0.5243	2.5134	2.9917	−0.0962	0.4269	0.7796	−0.0113	1.1086	1.5550	−0.0043	0.4683	0.7375
Triweight	LC	−0.5385	2.5014	2.9796	−0.0968	0.4410	0.7908	−0.0118	1.1175	1.5604	−0.0047	0.4822	0.7545
	QL	−0.5461	2.6572	3.1352	−0.0768	0.4508	0.8049	−0.0112	1.1052	1.5436	−0.0043	0.4872	0.7575
	DA via (12)	−0.4848	2.5690	3.0550	−0.0714	0.5009	0.8388	−0.0086	1.0881	1.5156	−0.0019	0.4891	0.7815
	CN via (13)	−0.5246	2.5143	2.9927	−0.0970	0.4263	0.7790	−0.0113	1.1086	1.5550	−0.0043	0.4687	0.7375
Uniform	LC	−0.5135	2.4450	2.9323	−0.1076	0.4441	0.7932	−0.0115	1.1237	1.5641	−0.0043	0.4817	0.7581
	QL	−0.5393	2.6181	3.0978	−0.0921	0.4632	0.8175	−0.0104	1.0977	1.5383	−0.0039	0.4940	0.7746
	DA via (12)	−0.4916	2.6213	3.1090	−0.0852	0.4962	0.8359	−0.0100	1.0909	1.5268	−0.0032	0.4913	0.7939
	CN via (13)	−0.4810	2.4469	2.9374	−0.1003	0.4339	0.7869	−0.0113	1.1263	1.5663	−0.0040	0.4759	0.7531

Note: Kernel and boundary condition configure the LPRF trend-cycle filter applied for extracting the day-of-the-year pattern. The considered boundary conditions are the so-called linear-constant (LC) and quadratic-linear (QL) assumptions, the direct asymmetric (DA) filters approach (12), and the cut-and-normalise (CN) approach (13). When estimating the day-of-the-week pattern, however, the exact Henderson kernel along with the LC boundary condition is always specified. Revision measures are the mean revision (MR), the mean absolute revision (MAR), and the standard deviation (SD) of the revisions. These measures have been calculated from the seasonally adjusted vintage consumption series released between W01 2022 and W52 2024, with final estimates being obtained from the 2025 W52 release vintage.

Table 4: Revisions in seasonally adjusted daily electricity consumption under RKHS trend-cycle estimation

		LCE revisions (8)						PGR revisions (9)					
		Final revisions $\{r_t\}$			Lag-1 revisions $\{r_t(1)\}$			Final revisions $\{r_t^{\%}\}$			Lag-1 revisions $\{r_t^{\%}(1)\}$		
Kernel	Bandwidth selection	MR	MAR	SD	MR	MAR	SD	MR	MAR	SD	MR	MAR	SD
Biweight	$h_{f,\Gamma}$ via (17)	−0.5165	2.4984	2.9768	−0.0991	0.4268	0.7766	−0.0112	1.1142	1.5530	−0.0041	0.4700	0.7349
	$h_{f,A}$ via (19)	−0.5022	2.4658	2.9505	−0.1047	0.4265	0.7803	−0.0114	1.1183	1.5550	−0.0039	0.4709	0.7423
	$h_{f,T}$ via (20)	−0.5058	2.4793	2.9602	−0.0985	0.4263	0.7753	−0.0111	1.1112	1.5484	−0.0041	0.4685	0.7319
	$h_f = 184$	−0.5144	2.4944	2.9734	−0.0976	0.4222	0.7722	−0.0107	1.1146	1.5558	−0.0040	0.4640	0.7261
Epanechnikov	$h_{f,\Gamma}$ via (17)	−0.5045	2.4757	2.9579	−0.1049	0.4316	0.7846	−0.0112	1.1161	1.5535	−0.0041	0.4755	0.7478
	$h_{f,A}$ via (19)	−0.4889	2.4585	2.9440	−0.1009	0.4270	0.7804	−0.0112	1.1169	1.5542	−0.0038	0.4712	0.7413
	$h_{f,T}$ via (20)	−0.4952	2.4629	2.9448	−0.1031	0.4298	0.7827	−0.0112	1.1132	1.5522	−0.0041	0.4745	0.7463
	$h_f = 184$	−0.5022	2.4720	2.9546	−0.1029	0.4288	0.7814	−0.0108	1.1182	1.5582	−0.0039	0.4720	0.7428
Henderson	$h_{f,\Gamma}$ via (17)	−0.4800	2.4389	2.9329	−0.1092	0.4308	0.7827	−0.0112	1.1286	1.5608	−0.0036	0.4782	0.7436
	$h_{f,A}$ via (19)	−0.4742	2.4455	2.9405	−0.1081	0.4311	0.7862	−0.0111	1.1275	1.5592	−0.0037	0.4781	0.7475
	$h_{f,T}$ via (20)	−0.4741	2.4319	2.9276	−0.1077	0.4307	0.7831	−0.0111	1.1271	1.5608	−0.0036	0.4787	0.7446
	$h_f = 184$	−0.4775	2.4378	2.9325	−0.1089	0.4284	0.7812	−0.0108	1.1301	1.5650	−0.0036	0.4711	0.7413
Triweight	$h_{f,\Gamma}$ via (17)	−0.5232	2.5104	2.9877	−0.0962	0.4237	0.7756	−0.0114	1.1069	1.5458	−0.0043	0.4659	0.7317
	$h_{f,A}$ via (19)	−0.5073	2.4757	2.9586	−0.1012	0.4252	0.7805	−0.0116	1.1161	1.5531	−0.0039	0.4734	0.7452
	$h_{f,T}$ via (20)	−0.5136	2.4894	2.9692	−0.0952	0.4230	0.7752	−0.0114	1.1052	1.5433	−0.0042	0.4659	0.7317
	$h_f = 184$	−0.5235	2.5092	2.9866	−0.0955	0.4198	0.7721	−0.0110	1.1080	1.5507	−0.0042	0.4615	0.7268
Uniform	$h_{f,\Gamma}$ via (17)	−0.4855	2.4478	2.9386	−0.1070	0.4297	0.7797	−0.0111	1.1259	1.5606	−0.0036	0.4756	0.7366
	$h_{f,A}$ via (19)	−0.4778	2.4496	2.9416	−0.1047	0.4290	0.7823	−0.0111	1.1257	1.5600	−0.0036	0.4748	0.7417
	$h_{f,T}$ via (20)	−0.4807	2.4416	2.9334	−0.1059	0.4288	0.7789	−0.0111	1.1249	1.5591	−0.0037	0.4752	0.7362
	$h_f = 184$	−0.4830	2.4468	2.9375	−0.1058	0.4276	0.7780	−0.0108	1.1286	1.5655	−0.0036	0.4695	0.7332

Note: Kernel and bandwidth selection configure the RKHS trend-cycle filter applied for extracting the day-of-the-year pattern, assuming a random walk input in the spectral optimality criteria. The considered criteria for deriving optimal bandwidths for asymmetric boundary kernels are the frequency response criterion (17), the accuracy criterion (19), and the timeliness criterion (20). When estimating the day-of-the-week pattern, however, the biweight kernel along with the frequency response criterion (17) under the random walk assumption is always specified. Revision measures are the mean revision (MR), the mean absolute revision (MAR), and the standard deviation (SD) of the revisions. These measures have been calculated from the seasonally adjusted vintage consumption series released between W01 2022 and W52 2024, with final estimates being obtained from the 2025 W52 release vintage.

RKHS trend-cycle filter that generally outperforms its competitors in terms of generating universally lower revisions in the seasonally adjusted vintage consumption series. The only general conclusion one might draw is that the revision profiles recorded under usage of the RKHS methodology seem slightly less volatile and less dependent on the derivation of boundary kernels than those obtained under usage of LPRF trend-cycle filters.

Looking closer at the numbers, we find that the initial level of the seasonally adjusted estimates commonly tends to be corrected downwards by about 0.1% after one week and by roughly 0.5% in the end, which translates into average downwards revisions in the initial day-on-day growth rates by about 0.004 percentage point after one week and by approximately 0.01 percentage point in the end. In absolute terms, the average LCE revision ranges between 0.42% and 0.50% after one week and eventually between 2.32% and 2.65%, whereas the average PGR revision lies roughly between 0.46 and 0.50 percentage point after one week and between 1.08 and 1.13 percentage points in the end. The standard deviation of the LCE revisions varies between 0.77 and 0.84 percentage point after one week and eventually between 2.92 and 3.14 percentage points, while the corresponding volatility bands for the PGR revisions are 0.73–0.80 and 1.54–1.57 percentage points, respectively. Finally, it is also noted (but not explicitly reported) that all revision measures tend to increase marginally when the trend-cycle filters used in the DOW and DOY estimation steps share the same kernel configuration, as initially foreseen in the study design.

5 Summary

The COVID-19 pandemic outbreak in early 2020 has forcefully accelerated a renewal process in official statistics that had been initiated by a general discussion about the role of national statistical agencies in an increasingly digitised world almost a decade earlier. In particular, the compilation, processing, and dissemination of daily and weekly economic time series has gained major momentum since that tumultuous time, including the much needed tailoring of established seasonal adjustment approaches to the peculiarities of sub-monthly data. One such example is a modification of the nonparametric X-11 method for monthly and quarterly time series. Compared with its classical ancestor, the modified method implements some interesting additions, such as parametric trend-cycle estimation with kernel-based filter families that can be constructed within local polynomials regression models or reproducing kernel Hilbert spaces. These enhancements, however, come at the expense of some simplifications, such as the unavailability of automatic selection procedures for both trend-cycle and seasonal filters.

The main goal of the present paper was to evaluate the current maturity status of the modified X-11 method. We first provided an exhaustive list of the conceptual differences between the classical and modified computing routines, which fall into four main categories: data pretreatment based upon linear time series regression models with ARIMA disturbances, trend-cycle estimation, replacement of extremes in the detrended data, and seasonal estimation. The effects of these differences were then assessed empirically, using real-time data on monthly production of capital goods in Germany. Our study revealed that the classical and modified pretreatment models often produce the same parameter estimates for data with an integer seasonal periodicity; nevertheless, minor discrepancies may occasionally arise due to the slightly different model estimation routines that can

in turn lead to diverging outcomes of the automatic outlier detection modules. Either way, restricting parametric trend-cycle estimation to the exact Henderson and biweight kernels, the seasonally adjusted vintage production series obtained from the two X-11 methods were very similar in general. However, the missing extreme-value correction in the final filtering stage of the modified X-11 routines provoked the occasional occurrence of significantly different growth rates near the sample boundaries. Our attention then shifted from monthly to sub-monthly time series that typically call for the specification of trend-cycle filters with longer bandwidths. Real-time data on weekly Google trends and daily electricity consumption in Germany was considered to find out whether the configuration of the kernel-based trend-cycle filter significantly affects the quality of the final seasonally adjusted estimates. Looking at various quality diagnostics as well as short- and long-term revision profiles, it eventually turned out that this configuration has little effect on the performance of the modified X-11 method.

Future work on this method should first and foremost integrate an automatic correction of ill-specified seasonal filters to get rid of the annoying error message that currently pops up whenever the input time series is too short for the given setting. Another urgent improvement is the incorporation of some extreme-value correction into the final filtering recursion. Afterwards, the maturity status could be reassessed, potentially including forecast extensions generated from the modified pretreatment model. Further nice-to-have features may be implemented in the long run. For example, a data-driven selection procedure for the kernel-based trend-cycle filters, or less options for their configuration, could be helpful for some users. Similarly, an automatic selection of seasonal filters may be warranted as well, see, for instance, the related discussion in Webel (2026). Enabling the application of period-specific seasonal filters in certain special cases could also be beneficial; for example, the extraction of the day-of-the-week pattern from the daily electricity consumption series may be improved by using one filter for Mondays through Fridays and another one for Saturdays and Sundays.

References

Ahlburg, D. A. (1984, July–September). Forecast Evaluation and Improvement Using Theil's Decomposition. *Journal of Forecasting 3*(3), 345–351. https://doi.org/10.1002/for.3980030313.

Alexandrov, T., S. Bianconcini, E. B. Dagum, P. Maass, and T. S. McElroy (2012). A Review of Some Modern Approaches to the Problem of Trend Extraction. *Econometric Reviews 31*(6), 593–624. https://doi.org/10.1080/07474938.2011.608032.

Aronszajn, N. (1950, May). Theory of Reproducing Kernels. *Transactions of the American Mathematical Society 68*(3), 337–404. https://doi.org/10.2307/1990404.

Berlinet, A. (1993, December). Hierarchies of Higher Order Kernels. *Probability Theory and Related Fields 94*(4), 489–504. https://doi.org/10.1007/BF01192560.

Berlinet, A. and C. Thomas-Agnan (2004). *Reproducing Kernel Hilbert Spaces in Probability and Statistics*. Boston: Kluwer Academic.

Bliemel, F. (1973, November). Theil's Forecast Accuracy Coefficient: A Clarification. *Journal of Marketing Research 10*(4), 444–446. https://doi.org/10.1177/002224377301000413.

Cebrián, E. and J. Domenech (2023). Is Google Trends a Quality Data Source? *Applied Economics Letters 30*(6), 811–815. https://doi.org/10.1080/13504851.2021.2023088.

Cebrián, E. and J. Domenech (2024, May). Addressing Google Trends Inconsistencies. *Technological Forecasting and Social Change 202*, Article 123318. https://doi.org/10.1016/j.techfore.2024.123318.

Dagum, E. B. and S. Bianconcini (2008, October). The Henderson Smoother in Reproducing Kernel Hilbert Space. *Journal of Business & Economic Statistics 26*(4), 536–545. https://doi.org/10.1198/073500107000000322.

Dagum, E. B. and S. Bianconcini (2013). A Unified View of Nonparametric Trend-Cycle Predictors Via Reproducing Kernel Hilbert Spaces. *Econometric Reviews 32*(7), 848–867. https://doi.org/10.1080/07474938.2012.690674.

Dagum, E. B. and S. Bianconcini (2015, September). A New Set of Asymmetric Filters for Tracking Short-Term Trend in Real-Time. *Annals of Applied Statistics 9*(3), 1433–1458. https://doi.org/10.1214/15-AOAS856.

Doherty, M. (2001, December). The Surrogate Henderson Filters in X-11. *Australian & New Zealand Journal of Statistics 43*(4), 385–392. https://doi.org/10.1111/1467-842X.00187.

European Commission (2020, August). Commission Implementing Regulation (EU) 2020/1197 of 30 July 2020. *Official Journal of the European Union: Series L (Legislation) 63*(271), 1–170. http://data.europa.eu/eli/reg_impl/2020/1197/oj.

Eurostat (2024). ESS Guidelines on Seasonal Adjustment. Publications Office of the European Union, Luxembourg. https://doi.org/10.2785/705102.

Eurostat (2025). NACE Rev. 2.1: Statistical Classification of Economic Activities in the European Union. Publications Office of the European Union, Luxembourg. https://doi.org/10.2785/155339.

Fenga, L. (2020, March). Filtering and Prediction of Noisy and Unstable Signals: The Case of Google Trends Data. *Journal of Forecasting 39*(2), 281–295. https://doi.org/10.1002/for.2626.

Findley, D. F., B. C. Monsell, W. R. Bell, M. C. Otto, and B.-C. Chen (1998, April). New Capabilities and Methods of the X-12-ARIMA Seasonal-Adjustment Program. *Journal of Business & Economic Statistics 16*(2), 127–152. https://doi.org/10.1080/07350015.1998.10524743.

Gasser, T. and H.-G. Müller (1979). Kernel Estimation of Regression Functions. In T. Gasser and M. Rosenblatt (Eds.), *Smoothing Techniques for Curve Estimation*, Volume 757 of *Lecture Notes in Mathematics*, pp. 23–68. Heidelberg: Springer. https://doi.org/10.1007/BFb0098489.

Gómez, V. and A. Maravall (2001). Automatic Modeling Methods for Univariate Series. In D. Peña, G. C. Tiao, and R. S. Tsay (Eds.), *A Course in Time Series Analysis*, pp. 171–201. New York: Wiley. https://doi.org/10.1002/9781118032978.ch7.

Granger, C. W. J. and P. Newbold (1973). Some Comments on the Evaluation of Economic Forecasts. *Applied Economics 5*(1), 35–47. https://doi.org/10.1080/00036847300000003.

Henderson, R. (1916). Note on Graduation by Adjusted Average. *Transactions of the Actuarial Society of America 17*(55), 43–48.

Kenny, P. B. and J. Durbin (1982, January). Local Trend Estimation and Seasonal Adjustment of Economic and Social Time Series. *Journal of the Royal Statistical Society: Series A (General) 145*(1), 1–28. https://doi.org/10.2307/2981420.

Kyung-Joon, C. and W. R. Schucany (1998, March). Nonparametric Kernel Regression Estimation Near Endpoints. *Journal of Statistical Planning and Inference 66*(2), 289–304. https://doi.org/10.1016/S0378-3758(97)00082-7.

Ladiray, D., J. Palate, G. L. Mazzi, and T. Proietti (2018). Seasonal Adjustment of Daily and Weekly Data. In G. L. Mazzi, D. Ladiray, and D. A. Riester (Eds.), *Handbook on Seasonal Adjustment*, Chapter 29, pp. 757–783. Luxembourg: Publications Office of the European Union.

Ladiray, D. and B. Quenneville (2001). *Seasonal Adjustment with the X-11 Method*, Volume 158 of *Lecture Notes in Statistics*. New York: Springer. https://doi.org/10.1007/978-1-4613-0175-2.

Ljung, G. M. (1993, January). On Outlier Detection in Time Series. *Journal of the Royal Statistical Society: Series B (Methodological) 55*(2), 559–567. https://doi.org/10.1111/j.2517-6161.1993.tb01924.x.

Loader, C. (1999). *Local Regression and Likelihood*. New York: Springer. https://doi.org/10.1007/b98858.

Lothian, J. (1978, October). The Identification and Treatment of Moving Seasonality in the X-11 Seasonal Adjustment Method. Research Paper 78-10-004, Seasonal Adjustment and Time Series Analysis Staff, Statistics Canada.

Macaulay, F. R. (1931). *The Smoothing of Time Series*. New York: National Bureau of Economic Research. https://www.nber.org/books-and-chapters/smoothing-time-series.

McElroy, T. S. (2010, September). A Nonlinear Algorithm for Seasonal Adjustment in Multiplicative Component Decompositions. *Studies in Nonlinear Dynamics & Econometrics 14*(4), Article 6. https://doi.org/10.2202/1558-3708.1756.

McElroy, T. S. (2011, November). A Nonparametric Method for Asymmetrically Extending Signal Extraction Filters. *Journal of Forecasting 30*(7), 597–621. https://doi.org/10.1002/for.1175.

McElroy, T. S. and A. Sutcliffe (2006, May). An Iterated Parametric Approach to Nonstationary Signal Extraction. *Computational Statistics & Data Analysis 50*(9), 2206–2231. https://doi.org/10.1016/j.csda.2005.07.008.

Musgrave, J. C. (1964). A Set of End Weights to End all End Weights. Working Paper, U.S. Department of Commerce, Bureau of the Census, Washington, D.C. https://www.census.gov/content/dam/Census/library/working-papers/1964/adrm/musgrave1964a.pdf.

Proietti, T. and A. Luati (2008, December). Real Time Estimation in Local Polynomial Regression, with Application to Trend-Cycle Analysis. *Annals of Applied Statistics 2*(4), 1523–1553. https://doi.org/10.1214/08-AOAS195.

Quartier-la-Tente, A. (2024, December). Improving Real-Time Trend Estimates Using Local Parametrization of Polynomial Regression Filters. *Journal of Official Statistics 40*(4), 685–715. https://doi.org/10.1177/0282423X241283207.

Quartier-la-Tente, A. (2025). *Real-Time Trend-Cycle Estimation with Moving Averages: Contributions to Business Cycle Analysis*. Ph. D. thesis, Nantes Université.

Shiskin, J., A. H. Young, and J. C. Musgrave (1967). The X-11 Variant of the Census Method II Seasonal Adjustment Program. Technical Paper No 15, U.S. Department of Commerce, Bureau of the Census, Washington, D.C. https://www.census.gov/content/dam/Census/library/working-papers/1967/adrm/shiskinyoungmusgrave1967.pdf.

Soukup, R. J. and D. F. Findley (1999). On the Spectrum Diagnostics Used by X-12-ARIMA to Indicate the Presence of Trading Day Effects after Modeling or Adjustment. In *ASA Proceedings of the Joint Statistical Meetings, Business and Economic Statistics Section*, pp. 144–149. Alexandria, VA: American Statistical Association.

Theil, H. (1958). *Economic Forecasts and Policy*. Amsterdam: North-Holland.

Webel, K. (2022). A Review of Some Recent Developments in the Modelling and Seasonal Adjustment of Infra-Monthly Time Series. Discussion Paper 31/2022, Deutsche Bundesbank, Frankfurt am Main. https://www.bundesbank.de/resource/blob/892512/5eb1bc37738d249c32599abefec32065/472B63F073F071307366337C94F8C870/2022-08-11-dkp-31-data.pdf.

Webel, K. (2025, June). Revisions in Concurrent Seasonal Adjustments of Daily and Weekly Economic Time Series. *Statistical Journal of the IAOS 41*(2), 265–293. https://doi.org/10.1177/18747655251341459.

Webel, K. (2026). Redesigning the Classical Automatic Selection of X-11 Seasonal Filters. Discussion Paper 07/2026, Deutsche Bundesbank, Frankfurt am Main. https://doi.org/10.71734/DP-2026-7.

Webel, K. and A. Smyk (2024, December). Seasonal Adjustment of Infra-Monthly Time Series with JDemetra+. *Journal of Official Statistics 40*(4), 783–828. https://doi.org/10.1177/0282423X241277602.

Wildi, M. (2005). *Signal Extraction: Efficient Estimation, 'Unit-Root'-Tests and Early Detection of Turning Points*, Volume 547 of *Lecture Notes in Economics and Mathematical Systems*. Heidelberg: Springer. https://doi.org/10.1007/b138291.

Wildi, M. and T. S. McElroy (2019, July–September). The Trilemma Between Accuracy, Timeliness and Smoothness in Real-Time Signal Extraction. *International Journal of Forecasting 35*(3), 1072–1084. https://doi.org/10.1016/j.ijforecast.2019.03.008.

Appendix

This technical appendix summarises the main theory underlying the kernel-based trend-cycle extraction approaches available in the modified X-11 method (see Section 2). Since these approaches are always applied to some estimate of the seasonally adjusted data (B6, C6, D6, and D11 in Figure 1), the subsequent discussion will generally be centred around a nonseasonal time series $\{z_t\}$ that is assumed to contain only trend-cyclical and irregular movements.

A Local polynomial regression filters

Trend-cycle extraction utilising local polynomial regression filters (LPRF) has been developed in Proietti and Luati (2008), see also Quartier-la-Tente (2024, 2025) for a recent illustration and details about the implementation in the {`rjd3filters`} R package.

Model and filters Let b denote the filter's local bandwidth and δ the polynomial trend degree to be preserved by the filter. Furthermore, let $f \in \{0, \dots, b\}$ be the number of future observations available after the current time point t. Now, consider the local time series regression

$$\mathbf{z}_t = \mathbf{X}_f \boldsymbol{\zeta} + \boldsymbol{\varepsilon}_t, \tag{10}$$

where $\mathbf{z}_t = (z_{t-b}, \dots, z_{t+f})^\top$ is the local window of observations from $\{z_t\}$ at time t,

$$\mathbf{X}_f = \begin{pmatrix} 1 & -f & f^2 & \cdots & (-f)^\delta \\ 1 & -(f-1) & (f-1)^2 & \cdots & [-(f-1)]^\delta \\ \vdots & \vdots & \vdots & \ddots & \vdots \\ 1 & f & f^2 & \cdots & f^\delta \end{pmatrix}$$

is the time-constant design matrix, $\boldsymbol{\zeta} = (\zeta_0, \dots, \zeta_\delta)^\top$ is a $(\delta + 1)$-dimensional vector of unknown regression coefficients, and $\boldsymbol{\varepsilon}_t = (\varepsilon_{t-b}, \dots, \varepsilon_{t+f})^\top$ is a local vector of zero-mean white-noise processes that are both mutually and serially uncorrelated (as well as mutually uncorrelated with the aforementioned irregular movements). Then, the weighted

least squares estimator of $\boldsymbol{\zeta}$ is found through minimising the objective function

$$\sum_{j=-b}^{f} \kappa_j \left(z_{t+j} - \zeta_0 - \zeta_1 j - \cdots - \zeta_\delta j^\delta \right)^2, \tag{11}$$

where $\{\kappa_j\}$ is a sequence of non-negative numbers, which represents the weights assigned to the residuals from model (10) and defines, either implicitly or explicitly, a kernel function. It follows from standard least squares estimation theory that this objective function is minimised for

$$\hat{\boldsymbol{\zeta}} = \left(\mathbf{X}_f^\top \mathbf{K}_f \mathbf{X}_f \right)^{-1} \mathbf{X}_f^\top \mathbf{K}_f \mathbf{z}_t,$$

where $\mathbf{K}_f = \text{diag}(\kappa_{-b}, \ldots, \kappa_f)$. Letting $\mathbf{e}_{k,n}$ be the k-th unit vector of length n, the local trend-cycle estimator can be written as $\hat{\zeta}_0 = \mathbf{e}_{1,\delta+1}^\top \hat{\boldsymbol{\zeta}}$, so that $\hat{\zeta}_0 = \mathbf{w}_f^\top \mathbf{z}_t$ with LPRF weights

$$\mathbf{w}_f = \mathbf{K}_f \mathbf{X}_f \left(\mathbf{X}_f^\top \mathbf{K}_f \mathbf{X}_f \right)^{-1} \mathbf{e}_{1,\delta+1}. \tag{12}$$

Assuming $2b \geq \delta$, the symmetric LPRF weights result from setting $f = b$ in (12), whereas the asymmetric variants can be obtained for any choice of $f \in \{0, \ldots, b-1\}$. Although the latter "direct" asymmetric (DA) filters are conceptually consistent with the symmetric LPRF filter, they often yield strongly localised and, hence, volatile trend-cycle estimates.

Alternative asymmetric filters Proietti and Luati (2008) also suggest a more sophisticated alternative that essentially aims at a classic bias-variance trade-off. Its key idea is to purposely introduce a slight bias into the asymmetric trend-cycle estimators by assuming that the polynomial trend degree of interest is of some lower order $\overline{\delta} < \delta$ near the sample boundaries and by seeking asymmetric filters $\mathbf{w}_f$ that preserve polynomials up to an even lower degree $\underline{\delta} < \overline{\delta}$ subject to the reproduction constraints dictated by the symmetric filter $\mathbf{w}_b$. Since we will be mainly interested in the preservation of cubic polynomials ($\delta = 3$), only the constant-constant, cubic-quadratic, linear-constant, and quadratic-linear asymmetric variants will be evaluated in this paper; their defining $(\overline{\delta}, \underline{\delta})$ combinations are stated in Table 6 and Table 7 below.

A much simpler alternative of obtaining the asymmetric filter weights $\mathbf{w}_f$ from the symmetric ones $\mathbf{w}_b$ is inspired by the "cut-and-normalise" (CN) approach originally introduced by Gasser and Müller (1979) in the context of kernel regression estimation; some asymptotic properties and convergence rates of such kernel-based estimators are studied in Kyung-Joon and Schucany (1998). Translated to our linear filtering problem, any asymmetric CN variant is found through trimming the unneeded last $b - f$ elements from the symmetric filter and dividing the remaining $b + f + 1$ weights by their sum, that is,

$$\mathbf{w}_f = \left[\mathbf{1}^\top \begin{pmatrix} \mathbf{I} & \mathbf{0} \end{pmatrix} \mathbf{w}_b \right]^{-1} \begin{pmatrix} \mathbf{I} & \mathbf{0} \end{pmatrix} \mathbf{w}_b, \tag{13}$$

where $\mathbf{I}$ is the $(b + f + 1)$-dimensional identity matrix, $\mathbf{0}$ is a $(b + f + 1) \times (b - f)$ matrix of zeros, and $\mathbf{1}$ is a $(b + f + 1)$-dimensional vector of ones.

B Reproducing kernel Hilbert spaces

The main theory of reproducing kernels and associated Hilbert spaces has been developed by Aronszajn (1950), see also Berlinet and Thomas-Agnan (2004) for a more recent outline. In essence, a reproducing kernel Hilbert space (RKHS) is a Hilbert space characterised by a kernel that reproduces every function of the space via an inner product. In what follows, we distill the key ideas of RKHS-based trend-cycle estimation, drawing predominantly from the elaboration in Dagum and Bianconcini (2008, 2013, 2015), but see also Alexandrov, Bianconcini, Dagum, Maass, and McElroy (2012) for a less technical overview and an empirical comparison with other modern approaches to trend-cycle extraction.

Symmetric filter Compared to the LPRF approach, we now require the additional assumption that the discrete input series $\{z_t\}$ is a finite realisation of a stochastic process, whose continuous trajectories $\{Z(t)\}_{t\in\mathbb{T}}$ are square Lebesgue integrable functions with respect to a density f_0 defined on some index set $\mathbb{T} \subseteq \mathbb{R}$, that is, $\int_{\mathbb{T}} |Z(t)|^2 f_0(t)\, dt < \infty$. In other words, we assume that $Z \in \mathcal{L}^2(f_0)$, where $\mathcal{L}^2(f_0)$ is the Hilbert space of square Lebesgue integrable functions, equipped with the inner product

$$\langle Z_1, Z_2 \rangle_{\mathcal{L}^2(f_0)} = \int_{\mathbb{T}} Z_1(t) Z_2(t) f_0(t)\, dt$$

for all functions $Z_1, Z_2 \in \mathcal{L}^2(f_0)$. Reconsidering the local polynomial approximation (10) for the symmetric case ($f = b$), the trend signal inherent in $\{z_t\}$ can then be analysed within the space of polynomials of degrees up to δ, $\mathcal{P}_\delta \subseteq \mathcal{L}^2(f_0)$. The minimisation problem corresponding to the time-discrete objective function (11) thus reads

$$\min_{\zeta\in\mathcal{P}_\delta} ||Z - \zeta||^2_{\mathcal{P}_\delta} = \int_{\mathbb{T}} [Z(t-s) - \zeta(t-s)]^2 f_0(s)\, ds,$$

where $||\cdot||^2_{\mathcal{P}_\delta}$ is the $\mathcal{P}_\delta$-norm. Its unique solution is given by

$$\hat{\zeta}(t) = \int_{\mathbb{T}} Z(t-s)\, \kappa_{\delta+1}(s)\, ds,$$

where $\kappa_{\delta+1}$ denotes a kernel function of degree $\delta+1$. Assuming $\delta \geq 1$ and f_0 having finite moments up to order 2δ, Berlinet (1993) showed that $\kappa_{\delta+1}(t) = \kappa^\star_\delta(t,0) f_0(t)$, where $\kappa^\star_\delta(t,\cdot)$ is the reproducing kernel of $\mathcal{P}_\delta$; the latter can be constructed either from any sequence of $\delta+1$ orthonormal polynomials in $\mathcal{L}^2(f_0)$ or, equivalently, from the Hankel matrix storing the moments of f_0. Returning to discrete time, the RKHS analogue of the symmetric local polynomial trend-cycle filter (12) can be written as $\hat{\zeta}_0 = \tilde{\mathbf{w}}_b^\top \mathbf{z}_t$ with weights given by

$$\tilde{w}_{b,i} = \frac{\kappa_{\delta+1}(i/h)}{\sum_{j=-b}^{b} \kappa_{\delta+1}(j/h)}, \quad i \in \{-b, \ldots, b\}, \tag{14}$$

where h is a time-invariant global bandwidth parameter that should guarantee non-zero weights for only the $2b+1$ neighbouring observations of the current target point. Dagum and Bianconcini (2008, 2013) set this parameter to $h = b + 1$.

Asymmetric filters The corresponding asymmetric weights $\tilde{\mathbf{w}}_f$ for $f \in \{0, \dots, b-1\}$ can be easily obtained within the RKHS framework by simply adapting the kernel function $\kappa_{\delta+1}$ in (14) to the length of the requisite asymmetric filter. Following the CN approach, Dagum and Bianconcini (2008, 2013) construct boundary kernels with an appropriately truncated support $\underline{\mathbb{T}} \subset \mathbb{T}$ according to

$$\kappa_{\delta+1}^{(f)}(t) = \kappa_{\delta+1}(t) \times \left[\int_{\underline{\mathbb{T}}} \kappa_{\delta+1}(s)\, ds \right]^{-1},$$

so that the asymmetric weights $\tilde{\mathbf{w}}_f$ can be calculated in line with (14) as

$$\tilde{w}_{f,i} = \frac{\kappa_{\delta+1}^{(f)}(i/h_f)}{\sum_{j=-b}^{f} \kappa_{\delta+1}^{(f)}(j/h_f)}, \quad i \in \{-b, \dots, f\}, \tag{15}$$

where h_f is now a time-varying local bandwidth parameter, that is, h_f is specific to the boundary kernel $\kappa_{\delta+1}^{(f)}$; nevertheless, they conveniently use $h_f = h = b+1$. Using the aforementioned Hankel matrix, Dagum and Bianconcini (2015) derive a matrix representation for both the symmetric RKHS weights (14) and their asymmetric variants (15).

Optimal bandwidth selection for boundary kernels Dagum and Bianconcini (2015) also derive three spectral criteria for the optimal selection of the local bandwidth h_f; to this end, they translate the time domain minimisation problem of Musgrave (1964) into the frequency domain. Let $\Gamma(\omega) = \sum_j w_j \exp(-ij\omega)$ with $\omega \in [-\pi, \pi]$ be the frequency response function (FRF) of a linear filter defined through a potentially bi-infinite sequence of weights $\{w_j\}$; furthermore, let Γ_b and Γ_f denote the FRF of the symmetric and asymmetric RKHS filter defined through (14) and (15), respectively. Then, the mean squared revision error in the estimated trend-cycle that occurs when transitioning from any asymmetric to the symmetric RKHS filter, is given by

$$\frac{1}{2\pi} \int_{-\pi}^{\pi} |\Gamma_f(\omega) - \Gamma_b(\omega)|^2 f_z(\omega)\, d\omega, \tag{16}$$

where f_z is the (pseudo-)spectral density of the input series $\{z_t\}$. Accordingly, the optimal local bandwidth of the asymmetric RKHS filter in the FRF sense is obtained as

$$h_{f,\Gamma} = \min_{h_f} \int_{0}^{\pi} |\Gamma_f(\omega) - \Gamma_b(\omega)|^2 f_z(\omega)\, d\omega. \tag{17}$$

Dagum and Bianconcini (2015) also suggest two alternative selection criteria that emphasise the gain and phase properties of the involved filters. The gain function of a linear filter is generally defined as $G(\omega) = |\Gamma(\omega)|$, whereas the phase function is given by $\phi(\omega) = \mathrm{Arg}\,[\Gamma(\omega)]$. Bearing in mind that the latter vanishes for a symmetric filter, i.e. $\phi_b(\omega) \in \{0, \pm\pi\}$ in our case, the mean squared revision error (16) can be dissected into

two additive error contributions according to

$$\int_{-\pi}^{\pi} |\Gamma_f(\omega) - \Gamma_b(\omega)|^2 f_z(\omega)\, d\omega = \int_{-\pi}^{\pi} [G_f(\omega) - G_b(\omega)]^2 f_z(\omega)\, d\omega + 2\int_{-\pi}^{\pi} G_f(\omega) G_b(\omega) \{1 - \cos[\phi_f(\omega)]\} f_z(\omega)\, d\omega. \tag{18}$$

Dagum and Bianconcini (2015) construct one bandwidth selection criterion from each error contribution. The modified X-11 method, however, implements the three closely related optimality criteria advocated in Wildi and McElroy (2019), which relate to the accuracy, timeliness, and smoothness properties of the asymmetric filter. To this end, appropriate pass- and stop-bands have to be specified; since we are dealing with a trend-cycle extraction problem here, we define the pass-band as $[0, \underline{\omega}]$ for some $\underline{\omega} \in (0, \pi)$ and the stop-band as $(\underline{\omega}, \pi]$. The accuracy criterion, which measures the mean squared revision error contribution when both time displacement and noise suppression in the stop-band are ignored, is then given by

$$h_{f,A} = \min_{h_f} \int_0^{\underline{\omega}} [G_f(\omega) - G_b(\omega)]^2 f_z(\omega)\, d\omega. \tag{19}$$

The timeliness criterion, which accounts for the contribution to (16) stemming from the time displacement introduced by the asymmetric filter, is defined as

$$h_{f,T} = \min_{h_f} 2\int_0^{\underline{\omega}} G_f(\omega) G_b(\omega) \{1 - \cos[\phi_f(\omega)]\} f_z(\omega)\, d\omega. \tag{20}$$

Finally, the smoothness criterion, which targets leakage effects of the asymmetric filter in the stop-band, is given by

$$h_{f,S} = \min_{h_f} \int_{\underline{\omega}}^{\pi} [G_f(\omega) - G_b(\omega)]^2 f_z(\omega)\, d\omega. \tag{21}$$

Note that it follows directly from (18) that, up to monotonic transformations, minimising the summed objective functions from (19) and (21) yields the gain criterion of Dagum and Bianconcini (2015), whereas (20) coincides with their phase criterion. In practice, the spectral density f_z appearing in each bandwidth selection criterion could be replaced with a nonparametric or model-based estimator $\hat{f}_z$; for the sake of convenience, however, the modified X-11 method implements just two generic density functions under the assumption that $\{z_t\}$ is either white noise (WN) or a random walk (RW), leading to $f_z(\omega) = 1$ in the former case and to $f_z(\omega) = \{2[1 - \cos(\omega)]\}^{-1}$ in the latter case.

C Direct filter approach

The construction of asymmetric boundary filters in the RKHS methodology is essentially organised in two steps. First, the optimal bandwidth h_f of each boundary kernel $\kappa_{\delta+1}^{(f)}$ is determined, potentially using one of the various spectral optimality criteria; second, the weights $\tilde{\mathbf{w}}_f$ of each asymmetric filter are calculated based upon the choice of h_f via (15). One could thus argue that the RKHS approach takes a detour. The direct filter

approach (DFA), which has first been introduced in Wildi (2005), seeks to obtain the ideal asymmetric filter weights by minimising the mean squared error criterion (16) directly over filter weights, rather than local bandwidths. To this end, the symmetric filter is seen as a target that the asymmetric filter attempts to approximate as closely as possible. Exploiting the revision error decomposition (18) yet again, the DFA minimisation criterion is given by

$$\begin{aligned}\mathbf{w}_{f,ATS} = \min_{\mathbf{w}_f} \alpha_A &\int_0^{\underline{\omega}} [G_f(\omega) - G_b(\omega)]^2 f_z(\omega)\, d\omega \\ &+ 2\alpha_T \int_0^{\underline{\omega}} G_f(\omega) G_b(\omega) \left\{1 - \cos\left[\phi_f(\omega)\right]\right\} f_z(\omega)\, d\omega \\ &+ \alpha_S \int_{\underline{\omega}}^{\pi} [G_f(\omega) - G_b(\omega)]^2 f_z(\omega)\, d\omega,\end{aligned} \tag{22}$$

where $(\alpha_A, \alpha_T, \alpha_S) \in [0,1]^3$ with $\alpha_A + \alpha_T + \alpha_S = 1$ is a weighting scheme that enables users to prioritise the accuracy, timeliness, and smoothness criteria.

D Kernel-based representations of the classical Henderson and Musgrave filters

This broad variety of options for constructing kernel-based trend-cycle filters and for deriving their asymmetric variants naturally raises the question which configuration provides the best approximation of the classical Henderson filter and its asymmetric Musgrave surrogates. To get an idea, we now calculate the weights of the symmetric and concurrent LPRF and RKHS filters with bandwidths $b \in \{4, 6, 11\}$ for all kernels $\{\kappa_j\}$ and derivation principles available in the modified X-11 method, and compare those to the weights of the classical benchmark filters. For the sake of brevity, however, we discuss only the results for $b = 6$ (and $\delta = 3$), as this is the most relevant case for our empirical maturity assessment in Section 3. Nevertheless, it should be generally kept in mind that the RKHS filters developed by Dagum and Bianconcini (2008, 2013, 2015) do not provide exact replications of but approximations to the classical Henderson and Musgrave filters. An alternative derivation of the exact asymmetric Musgrave variants using the RKHS methodology is discussed in Section 3.1 of Proietti and Luati (2008).

Table 5 reports the weights of the symmetric classical and kernel-based 13-term Henderson filters; the LPRF weights $\mathbf{w}_6$ have been obtained through (12), whereas the weights $\tilde{\mathbf{w}}_6$ of the RKHS filters have been calculated via (14). It is seen that the classical Henderson filter can be exactly replicated within the LPRF framework when using the (normalised) Henderson kernel defined through the discrete sequence $\{\kappa_j\}$ with

$$\kappa_j = \left[1 - \frac{j^2}{(b+1)^2}\right]\left[1 - \frac{j^2}{(b+2)^2}\right]\left[1 - \frac{j^2}{(b+3)^2}\right], \quad j \in \{-b, \dots b\},$$

see Proietti and Luati (2008) for details. Good LPRF approximations are also obtained with the biweight and tricube kernels, whereas the trapezoidal and uniform kernels provide rather poor approximations. The RKHS methodology does not allow for an exact replication of the classical 13-term Henderson filter; nevertheless, the exact Henderson

Table 5: Weights of the symmetric kernel-based 13-term Henderson filters available in the modified X-11 method

		Weight applied to position ...						
Method	Kernel	$t \pm 6$	$t \pm 5$	$t \pm 4$	$t \pm 3$	$t \pm 2$	$t \pm 1$	t
LPRF	Biweight	−0.01997	−0.03006	0.00195	0.07003	0.14934	0.21137	0.23467
	Gaussian	−0.03034	−0.02117	0.01196	0.07142	0.14500	0.20724	0.23175
	Henderson	−0.01936	−0.02786	0	0.06549	0.14736	0.21434	0.24006
	Parabolic	−0.04202	−0.02327	0.02909	0.09285	0.15073	0.19040	0.20444
	Trapezoidal	−0.04777	−0.02773	0.04160	0.10632	0.15254	0.18028	0.18952
	Triangular	−0.03154	−0.02226	0.01670	0.07421	0.13915	0.20037	0.24675
	Tricube	−0.01525	−0.03575	−0.00400	0.07435	0.15681	0.21040	0.22690
	Triweight	−0.00832	−0.02689	−0.01576	0.04693	0.14309	0.22920	0.26352
	Uniform	−0.07692	0	0.06294	0.11189	0.14685	0.16783	0.17483
RKHS	Biweight	−0.01986	−0.02982	0.00217	0.07010	0.14921	0.21106	0.23429
	Epanechnikov	−0.03759	−0.01851	0.03181	0.09254	0.14748	0.18508	0.19838
	Henderson	−0.01888	−0.02692	0.00094	0.06585	0.14681	0.21299	0.23840
	Triangular	−0.02885	−0.01900	0.01900	0.07460	0.13723	0.19634	0.24138
	Triweight	−0.00834	−0.02698	−0.01589	0.04685	0.14313	0.22937	0.26374
	Uniform	−0.03297	0.02198	0.06693	0.10190	0.12687	0.14186	0.14685
Henderson		−0.01936	−0.02786	0	0.06549	0.14736	0.21434	0.24006

Note: The Henderson method replicates the symmetric weights of the classical Henderson filter as given in Table 3.8 of Ladiray and Quenneville (2001).

Table 6: Weights of the concurrent Henderson kernel Musgrave filters available in the modified X-11 method

		Weight applied to position ...						
Method	Asymmetric variant	$n-6$	$n-5$	$n-4$	$n-3$	$n-2$	$n-1$	n
LPRF	DA via (12)	−0.01724	0.02189	0.04000	−0.03415	−0.09789	0.13220	0.95518
	CC via $(\overline{\delta}, \underline{\delta}) = (0, 0)$	0.03493	0.02642	0.05428	0.11977	0.20164	0.26862	0.29434
	LC via $(\overline{\delta}, \underline{\delta}) = (1, 0)$	−0.09186	−0.05811	0.01202	0.11977	0.24390	0.35315	0.42113
	QL via $(\overline{\delta}, \underline{\delta}) = (2, 1)$	0.11027	−0.08716	−0.14992	−0.07678	0.11101	0.38219	0.71040
	CQ via $(\overline{\delta}, \underline{\delta}) = (3, 2)$	−0.04191	0.09317	0.01352	−0.09930	−0.08621	0.20187	0.91886
	CN via (13)	−0.03121	−0.04494	0	0.10563	0.23766	0.34569	0.38717
	$\mathbf{w}_{0,ATS}$ via (22), $\{z_t\} = \text{WN}$	−0.05112	0.10329	0.02303	−0.10259	−0.09649	0.19891	0.92497
	$\mathbf{w}_{0,ATS}$ via (22), $\{z_t\} = \text{RW}$	−0.02078	0.05056	−0.00847	−0.05620	0.02545	0.02343	0.98601
RKHS	$h_{0,\Gamma}$ via (17), $\{z_t\} = \text{WN}$	−0.01618	0.02438	0.08470	0.15344	0.21652	0.26066	0.27649
	$h_{0,\Gamma}$ via (17), $\{z_t\} = \text{RW}$	0	−0.03992	−0.04054	0.05414	0.21876	0.37262	0.43493
	$h_{0,A}$ via (19), $\{z_t\} = \text{WN}$	−0.03362	−0.00279	0.06125	0.14538	0.22868	0.28944	0.31166
	$h_{0,A}$ via (19), $\{z_t\} = \text{RW}$	−0.03554	−0.00723	0.05677	0.14337	0.23040	0.29438	0.31785
	$h_{0,T}$ via (20), $\{z_t\} = \text{WN}$	0	−0.03992	−0.04054	0.05414	0.21876	0.37262	0.43493
	$h_{0,T}$ via (20), $\{z_t\} = \text{RW}$	0	−0.03992	−0.04054	0.05414	0.21876	0.37262	0.43493
	$h_{0,S}$ via (21), $\{z_t\} = \text{WN}$	0.02799	0.06828	0.11311	0.15654	0.19266	0.21654	0.22488
	$h_{0,S}$ via (21), $\{z_t\} = \text{RW}$	0.01008	0.05248	0.10395	0.15653	0.20175	0.23224	0.24299
	$h_0 = b + 1 = 7$	−0.03049	−0.04348	0.00152	0.10635	0.23710	0.34398	0.38501
	$\tilde{\mathbf{w}}_{0,ATS}$ via (22), $\{z_t\} = \text{WN}$	−0.05106	0.10316	0.02304	−0.10246	−0.09647	0.19876	0.92504
	$\tilde{\mathbf{w}}_{0,ATS}$ via (22), $\{z_t\} = \text{RW}$	−0.00970	0.02485	−0.00989	−0.01503	0.00134	0.01587	0.99255
Musgrave		−0.09186	−0.05811	0.01202	0.11977	0.24390	0.35315	0.42113

Notes: **1** The DFA criterion (22) utilises the symmetric Henderson LPRF filter $\mathbf{w}_6$ and RKHS filter $\tilde{\mathbf{w}}_6$, respectively, as the target filter and $\alpha_A = \alpha_T = \alpha_S = 1/3$. **2** The RKHS optimal boundary bandwidths are searched for over values of h_0 that ensure the concurrent filter $\tilde{\mathbf{w}}_0$ has length between $b = 6$ and $2b = 12$. The pass-band in (19) through (22) is defined through $\underline{\omega} = \pi/6$. **3** The Musgrave method replicates the asymmetric weights of the classical concurrent Musgrave filter as given in Table 3.8 of Ladiray and Quenneville (2001).

Table 7: Weights of the concurrent biweight kernel Musgrave filters available in the modified X-11 method

		Weight applied to position ...						
Method	Asymmetric variant	$n-6$	$n-5$	$n-4$	$n-3$	$n-2$	$n-1$	n
LPRF	DA via (12)	−0.01848	0.02411	0.04172	−0.03835	−0.09914	0.13680	0.95335
	CC via $(\overline{\delta}, \underline{\delta}) = (0, 0)$	0.03470	0.02461	0.05662	0.12469	0.20401	0.26604	0.28933
	LC via $(\overline{\delta}, \underline{\delta}) = (1, 0)$	−0.09335	−0.06076	0.01393	0.12469	0.24670	0.35141	0.41739
	QL via $(\overline{\delta}, \underline{\delta}) = (2, 1)$	0.11155	−0.09009	−0.15008	−0.07443	0.11202	0.38074	0.71029
	CQ via $(\overline{\delta}, \underline{\delta}) = (3, 2)$	−0.04092	0.09088	0.01379	−0.09723	−0.08605	0.19977	0.91977
	CN via (13)	−0.03234	−0.04869	0.00316	0.11343	0.24192	0.34239	0.38013
	$\mathbf{w}_{0,ATS}$ via (22), $\{z_t\} = \text{WN}$	−0.05099	0.10277	0.02364	−0.10238	−0.09748	0.19966	0.92478
	$\mathbf{w}_{0,ATS}$ via (22), $\{z_t\} = \text{RW}$	−0.00922	0.02339	−0.00881	−0.01424	0.00001	0.01633	0.99254
RKHS	$h_{0,\Gamma}$ via (17), $\{z_t\} = \text{WN}$	−0.01874	0.02521	0.08774	0.15620	0.21710	0.25884	0.27365
	$h_{0,\Gamma}$ via (17), $\{z_t\} = \text{RW}$	0	−0.04341	−0.04416	0.06036	0.22609	0.37190	0.42922
	$h_{0,A}$ via (19), $\{z_t\} = \text{WN}$	−0.03703	−0.00159	0.06636	0.15029	0.22972	0.28599	0.30626
	$h_{0,A}$ via (19), $\{z_t\} = \text{RW}$	−0.03914	−0.00605	0.06227	0.14876	0.23159	0.29063	0.31195
	$h_{0,T}$ via (20), $\{z_t\} = \text{WN}$	0	−0.04341	−0.04416	0.06036	0.22609	0.37190	0.42922
	$h_{0,T}$ via (20), $\{z_t\} = \text{RW}$	0	−0.04341	−0.04416	0.06036	0.22609	0.37190	0.42922
	$h_{0,S}$ via (21), $\{z_t\} = \text{WN}$	0.03097	0.07207	0.11600	0.15727	0.19081	0.21265	0.22023
	$h_{0,S}$ via (21), $\{z_t\} = \text{RW}$	0.00771	0.05244	0.10531	0.15799	0.20239	0.23191	0.24225
	$h_0 = b + 1 = 7$	−0.03217	−0.04833	0.00351	0.11359	0.24177	0.34199	0.37964
	$\tilde{\mathbf{w}}_{0,ATS}$ via (22), $\{z_t\} = \text{WN}$	−0.05098	0.10274	0.02364	−0.10235	−0.09747	0.19962	0.92480
	$\tilde{\mathbf{w}}_{0,ATS}$ via (22), $\{z_t\} = \text{RW}$	−0.00918	0.02329	−0.00878	−0.01418	0.00002	0.01625	0.99258
Musgrave		−0.09186	−0.05811	0.01202	0.11977	0.24390	0.35315	0.42113

Notes: **1** The DFA criterion (22) utilises the symmetric biweight LPRF filter $\mathbf{w}_6$ and RKHS filter $\tilde{\mathbf{w}}_6$, respectively, as the target filter and $\alpha_A = \alpha_T = \alpha_S = 1/3$. **2** The RKHS optimal boundary bandwidths are searched for over values of h_0 that ensure the concurrent filter $\tilde{\mathbf{w}}_0$ has length between $b = 6$ and $2b = 12$. The pass-band in (19) through (22) is defined through $\underline{\omega} = \pi/6$. **3** The Musgrave method replicates the asymmetric weights of the classical concurrent Musgrave filter as given in Table 3.8 of Ladiray and Quenneville (2001).

and biweight kernels give close approximations yet again, confirming an earlier finding of Dagum and Bianconcini (2008). These authors also prove that the continuous exact Henderson kernel density is given by

$$f_{0H}(t) = \frac{b+1}{\bar{\kappa}_T}\,\kappa_T[(b+1)\,t]\,\mathbb{I}_{[-1,1]}(t),$$

where $\kappa_T(x) = 35/32\,(1-x^2)^3$ is the triweight kernel density over the support $[-1,1]$, $\bar{\kappa}_T = \int_{-(b+1)}^{b+1} \kappa_T(j)\,dj$ with $j = (b+1)\,t$, and $\mathbb{I}_{\mathbb{T}}$ denotes the indicator function over the index set $\mathbb{T}$. They also derive the continuous biweight (second-order) kernel density as

$$f_{0B}(t) = \frac{15}{16}\left(1-t^2\right)^2 \mathbb{I}_{[-1,1]}(t).$$

The worst RKHS approximations of the classical 13-term Henderson filter are obtained from the Epanechnikov and uniform kernels.

Table 6 and Table 7 report the weights of the concurrent 7-term classical and kernel-based Musgrave filters, using the exact Henderson and biweight kernels, respectively, and the various LPRF and RKHS approaches to deriving asymmetric boundary filters. The concurrent DFA filters, obtained from (22) with $\alpha_A = \alpha_T = \alpha_S = 1/3$, are also shown.

Unsurprisingly, the classical Musgrave filter is exactly replicated within the LPRF framework when using the exact Henderson kernel under the linear-constant (LC) boundary assumption, which is basically a mere image of the classical Musgrave assumption. Both the concurrent LC filter constructed from the biweight kernel and, in general, the CN approach (13) also yield acceptable approximations. In contrast, the concurrent filters obtained either under the cubic-quadratic (CQ) and quadratic-linear (QL) boundary assumptions or directly via (12) are strongly localised and, hence, give rather poor approximations, regardless of the chosen kernel. Similarly, the weights of the concurrent filter obtained under the constant-constant (CC) boundary assumption display a rather flat profile and fail to mirror the characteristic negative entries at the early positions of the classical Musgrave filter.

Unfortunately, there is no universally best RKHS approximation of the concurrent classical Musgrave filter. When prioritising the most recent weights, the concurrent RKHS filters obtained via the FRF criterion (17) under the RW assumption or, equivalently, via the timeliness criterion (20) under both the WN and RW assumption provide a good approximation for either kernel. In particular, the most recent weight is $\tilde{w}_{0,0} \approx 0.43$ and, hence, very close to the Musgrave benchmark (0.42). However, $\tilde{w}_{0,-6} = 0$ in this case, so these concurrent filters are essentially 6-term filters. When prioritising the earlier weights, the concurrent RKHS filter obtained from simply setting $h_0 = b+1 = 7$ in (15), as done by Dagum and Bianconcini (2008, 2013), provides a more convenient approximation, despite $\tilde{w}_{0,0} \approx 0.38$ now. Applying the accuracy criterion (19) tends to result in mediocre approximations of the concurrent Musgrave filter, irrespective of the chosen kernel and the WN versus RW assumption on the input series. When using the smoothness criterion (21), the quality of the approximation becomes even worse; the resulting weights are reminiscent of the concurrent CC filters in the LPRF framework, having relatively flat profiles with $\tilde{w}_{0,-6} > 0$ and $\tilde{w}_{0,-5} > 0$. Overall, the biweight kernel seems to be slightly preferable over the exact Henderson kernel within the RKHS framework, despite the fact

that the concurrent filter weights reported in Table 6 and Table 7 differ only marginally.

Finally, we note that the DFA method utilising $\alpha_A = \alpha_T = \alpha_S = 1/3$ in (22) also produces strongly localised concurrent filters, although other asymmetric DFA filters with $f > 0$ have weights that are much more balanced (the same goes for the aforementioned asymmetric CQ, DA, and QL filters in the LPRF framework).

E Additional plots

This section collects the three supplementary plots referenced in the main text.

- Figure 11 shows for each of the four extreme-value detection scenarios, which have been defined in Section 3, the kernel density estimates obtained from the 242 values of Theil's U_1 coefficient (7) between the classical final extreme-value corrected seasonal-irregular component (D9) and two corresponding components retrievable in the modified X-11 method: the uncorrected final seasonal-irregular component (D8) and the unimplemented proxy correction (D1/D7). As opposed to Figure 4, kernel-based trend-cycle estimation now utilises the RKHS methodology with the exact Henderson and biweight kernels and the frequency response criterion (17) for obtaining boundary kernels under the RW assumption.

- Figure 12 shows the $3 \times k$ seasonal filters that have been automatically selected by the redesigned moving seasonality ratio (Webel, 2026) for the 208 vintage Google searches with shortened sample spans starting in W01 2009 (Section 4). Complementing Figure 7, it is seen that omitting the first 5-year data segment results in

  (1) the selection of the 3×5 seasonal filter for much more vintage series, which, in turn, increases significantly the number of filter revisions over time, irrespective of the trend-cycle filter configuration, and

  (2) visibly more differences between the automatic filter choices obtained under the various trend-cycle filter configurations.

- Figure 13 shows additional kernel density estimates for the sample lag-52 autocorrelations obtained from the differenced logged seasonally adjusted weekly Google searches, using the shortened unadjusted vintage series released between W01 2022 and W52 2025. It thus complements Panel (d) of Figure 8 and highlights the fact that the various trend-cycle filter configurations now tend to have a stronger systematic effect on the quality of the seasonally adjusted estimates, compared to the full-samples case. These configurations particularly affect the shape of the estimated kernel densities, while their supports barely alter at all.

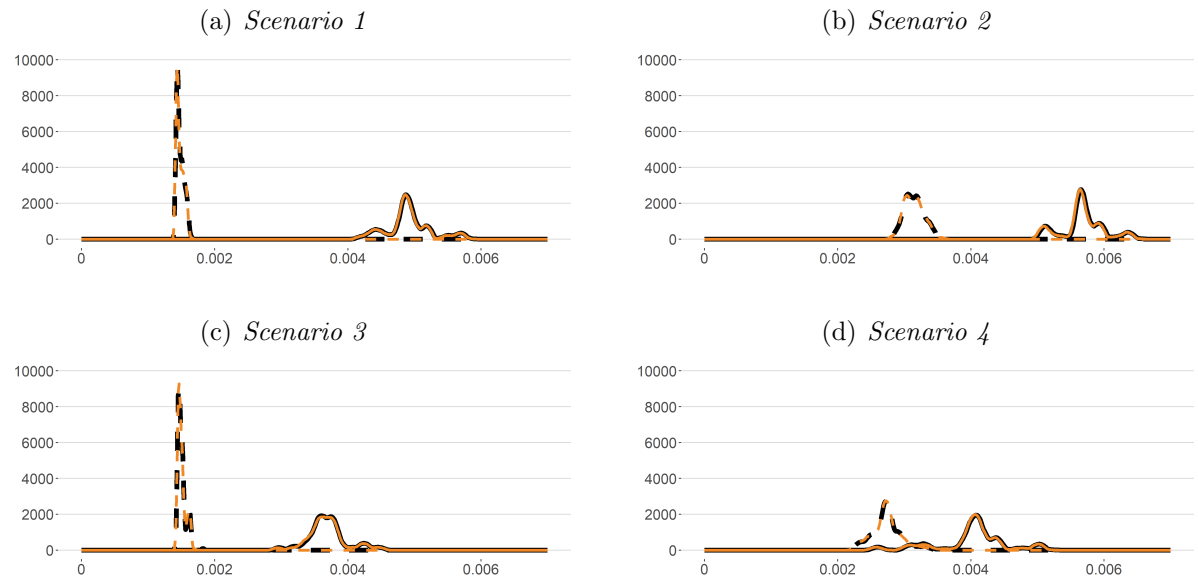


Figure 11: Epanechnikov kernel density estimates for Theil's U_1 coefficient (7) between the extreme-value corrected seasonal-irregular component (D9) from the classical X-11 method and related components from the modified X-11 method. The latter are the unmodified seasonal-irregular component (D8, *solid lines*) and its proxy correction (D1/D7, *dashed lines*); the modified X-11 method utilises reproducing kernel Hilbert spaces with the exact Henderson (*orange lines*) and biweight (*black lines*) kernels.

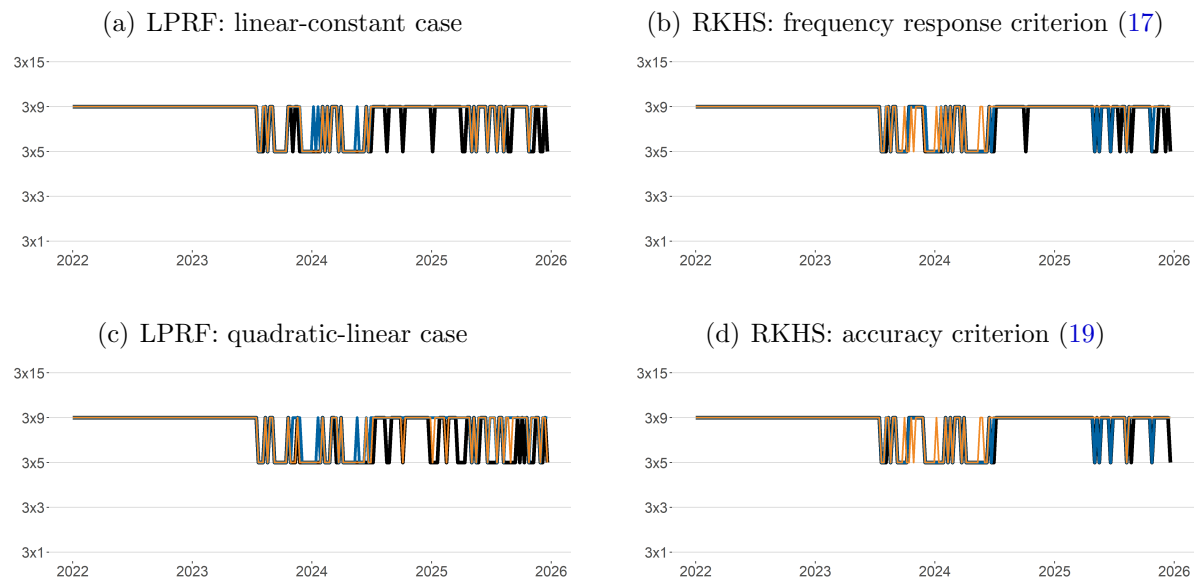


Figure 12: Automatic selection of $3 \times k$ seasonal filters for extracting the week-of-the-year pattern from the Google searches released in the W01 2022 through W52 2025 data vintages with starting date W01 2009. Panels (a) and (c) show the selected filters when using trend-cycle estimation based upon local polynomial regression filters with the Henderson (*black lines*), uniform (*blue lines*), and Gaussian (*orange lines*) kernels. Panels (b) and (d) show the selected filters when using trend-cycle estimation based upon reproducing kernel Hilbert spaces with the biweight (*black lines*), Epanechnikov (*blue lines*), and uniform (*orange lines*) kernels, where bandwidth selection for boundary kernels assumes a random walk in the specified optimality criteria.

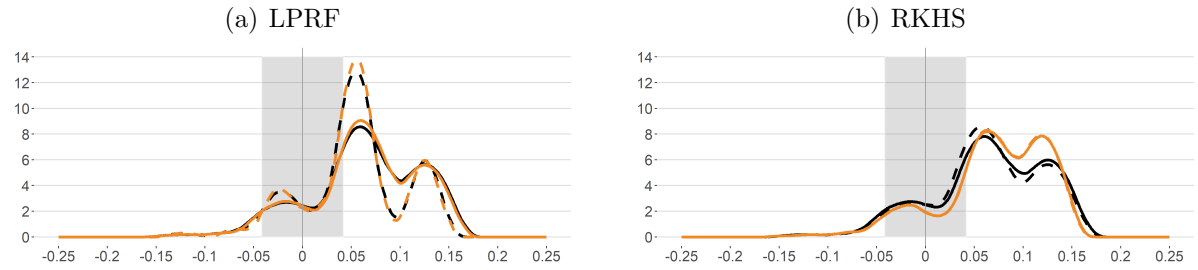


Figure 13: Epanechnikov kernel density estimates for $\hat{\rho}_{52}$ obtained from the differenced logged seasonally adjusted Google searches, using the W01 2022 through W52 2025 release vintages as of W01 2009 and automatically selected seasonal filters. In Panel (a), LPRF trend-cycle estimation is carried out with the biweight (*black lines*) and triangular (*orange lines*) kernels under the linear-constant boundary assumption (*solid lines*) and the direct approach (12) (*dashed lines*). In Panel (b), RKHS trend-cycle estimation is carried out with the triweight (*black lines*) and uniform (*orange lines*) kernels under the accuracy criterion (19) (*solid lines*) and the timeliness criterion (20) (*dashed lines*) with the random walk assumption.